Department of Precision and Microsystems Engineering

Focal plane flatness of an electrostatic lens

F.T. Overes

Report no : 2021.084
Coach : Dr. Ir. J.F.C. van Gurp
Professor : Ir. J.W. Spronck
Specialisation : MSD
Type of report : MSc Thesis report
Date : October 14, 2021

Summary

This research will evaluate whether the flatness requirements of a multibeam electrostatic lens can be met. First the subject is introduced with their use in scanning electron microscopes and why they need to be improved. Next the basic method of operation and general layout is shown and explained, see figure 1.
The introduction is followed by a system breakdown and boundary conditions. In this chapter the key requirement (the focal plane flatness) and the limiting boundary conditions of the lens are explained. The boundary conditions are limiting for most design choices in the lens. However, the choice of bonding method between the lens elements and spacer is not yet determined.
The choice in bonding method will be covered in the following chapter design choices. First the requirements and the possible methods of bonding are explained in detail. Next, the methods of bonding are compared to each other and the best solution is chosen. In this trade-off adhesive bonding is selected as the preferred method of bonding, therefore another trade-off is introduced to choose the most promising adhesive. The adhesive trade-off resulted in three possible adhesives that largely satisfy the requirements.
The flatness errors in the lens elements can mostly be compensated by changing certain parameters inside the SEM. In the next chapter the methods of compensation are explained and based on these methods the errors are divided in categories. The size of the error budget of these categories is based on how much can be compensated with each method. Next, the size of the expected errors for each category is calculated and it is estimated whether they fit in the available budgets. This resulted in some changes in volume claims and design of the lens, but with the changed conditions the budget is sufficient for the calculated errors. Unfortunately not all errors could be easily estimated with the available FEM software. Therefore, to estimate the size of the remaining errors some tests are proposed.
In the bonding trade-off the downsides of adhesives are listed. One of these downsides is the low resistance to temperature, which for adhesives depends on the glass transition temperature (Tg). The Tg is determined by the adhesive and the curing process. To test which adhesive in combination with which curing process results in the best Tg a test is proposed. The test showed that for 2 out of the 3 adhesives a higher curing temperature significantly improved the Tg, while for one adhesive it had little to no effect.
On top of the low temperature resistance adhesives are prone to drift under shear loads. The effect of drift on the element flatness error will be amplified. Therefore, this effect can have a very large influence on the caused bow errors. To estimate the effect of drift on the element flatness another test is proposed which will measure the drift of an element in similar conditions. The element is exposed to a similar load and suspension and the bow is measured over a period of about 2 months. A few adhesives were able to just fit in the available budget. In the last weeks of the measurement the amount of drift seems to stabilise, indicating that it might be possible to reach a steady state.

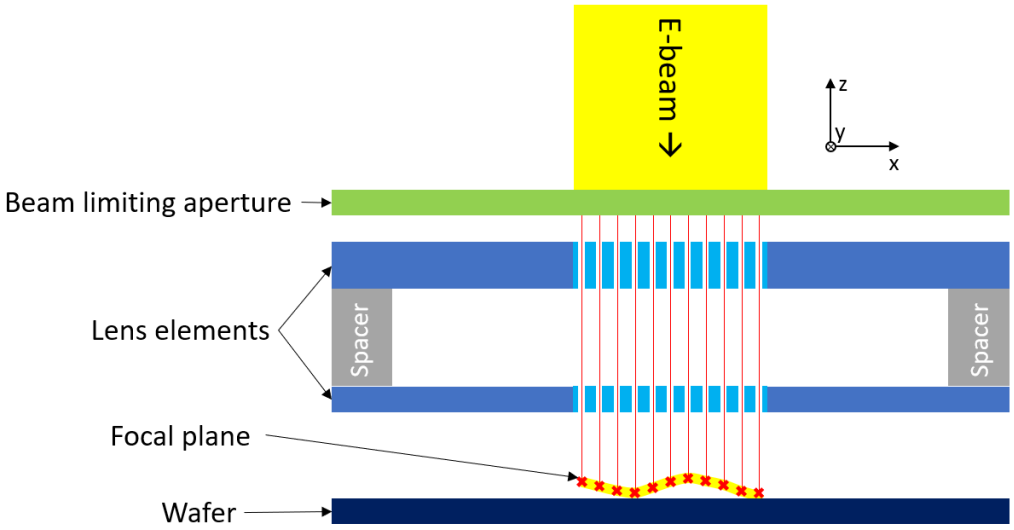

Figure 1: Schematic overview of an electrostatic lens setup, the lens elements form the system that is the topic of this report

1 Introduction

Moore's law claims that the number of transistors on a chip doubles every 2 years [1], this law has been upheld for the past 40 years largely due to the contribution of a Dutch company called ASML.
Chips are produced on a wafer in multiple steps, one of the most important steps of this process is lithography (projecting an image on a wafer), ASML specializes in the production of these machines. The lithography step will determine the size and position of the features. When these features are smaller more will fit on a chip, making the chip smaller, faster, cheaper and more efficient. The latest generation EUV scanners are able to reach a resolution of 13 nanometer. To achieve this precision very tight tolerances and ingenious methods are required, one of these methods is holistic lithography.
Holistic lithography uses data from previous wafers the improve the production process for the next batch. The size of the features that have to be measured are too small for conventional light based metrology systems. Therefore, to reach the required precision SEM's (Scanning Electron Microscopes) are used.
In this chapter the basics of (multibeam) scanning electron microscopes and electrostatic lenses are explained, as well as the layout of this report.

1.1 Scanning Electron Microscope

A scanning electron microscope (SEM) operates by shooting a beam of focused electrons on a sample. Upon impact, various signals are created that can be measured. Among them are secondary electrons, reflected/back scattered electrons and various wavelengths of light (typically X-ray). For imaging, secondary electrons are used, which are electrons that are knocked free when the electron beam impacts the sample. The amount of measured electrons determine the shade of the pixel, no secondary electrons create a black pixel, many electrons create a white pixel. A scanning electron microscope moves the beam over the sample in a pattern. Each secondary electron measurement, combined with the location of the beam, creates a pixel in the image.
This process requires a single beam to scan the entire wafer, which is rather time consuming. As holistic lithography requires the feedback of the first wafer before the machine can start on the second wafer, the lithography machines will stand still during the inspection. Therefore, it is of utmost importance that the inspection happens as fast as possible. To increase the speed of an SEM multiple beams can be used simultaneously, creating a multibeam SEM. Doubling the amount of beams will double the speed at which the machine operates, however it also increases the complexity. Each beam requires its own lens with its own focal point. If one of the focal points is not properly positioned on the sample a part of the image will be out of focus.

1.2 Electrostatic lenses

To achieve a proper image the electron beam has to be focused on the sample. This can be achieved by using an electrostatic aperture lens. By applying a potential difference between two plates an electric field is created, see Figure 3. This figure shows the equipotential lines of the electric field (blue) which are perpendicular to the electric field lines. When an electron passes through an electric field it will experience a force perpendicular to these equipotential lines (or along the electric field lines), the path of an electron is depicted with red lines. When the plates contain holes, the equipotential lines will bulge outwards, which will exert a force on the electrons that will focus the beam. The focal point of each beam in the electrostatic lens is determined by the strength of the field, geometry of the holes and position of the elements. Electrostatic lenses are in many aspects very comparable to optical lenses, however, there are a few differences. Due to the potential difference between the plates the lens will either accelerate or decelerate the electrons. An electrostatic lens is also unable to have a negative focal point (thus divergent lenses are not possible).

In a multibeam SEM lens there is not a single hole, but rather a grid of holes. Each of these holes is a lens with a single focus point, together these points form the focal plane. To achieve a sharp image the measured sample needs to be within a certain tolerance of the focal plane, this tolerance can be sub-micrometer. The goal of this research is to evaluate whether the required focal plane flatness for a multibeam SEM lens is achievable.

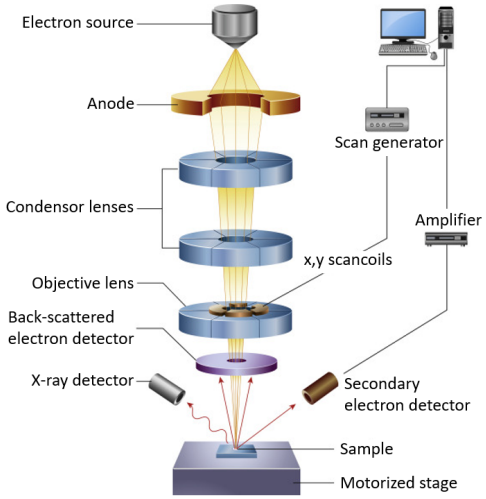

Figure 2: Schematic of a single beam SEM [5]

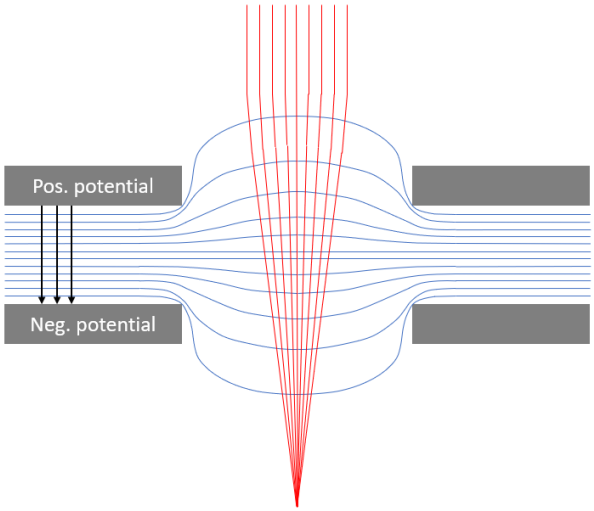

Figure 3: Electrostatic aperture lens

1.3 Layout of the report

This thesis report will start with a basic electrostatic lens setup, the key requirements and the boundary conditions. These subjects are explained in chapter 3. When the system layout and requirements are clear, choices can be made for the construction of the system. Therefore, a trade off between different bonding techniques and adhesives is covered in the chapter 4. Together, chapters 3 & 4 complete the full system overview.
In chapter 5 all expected errors are listed and for each of these errors the size is estimated with the help of FEM calculations. Some of these errors are difficult to calculate with FEM, therefore experiments are designed to quantify some of these errors. The objective, design and data analysis of these experiments is covered in chapter 6, followed by the results, discussion and recommendation for future research in chapter 7. Finally the report will finish with a conclusion. As this research contains valuable intellectual property from ASML some tolerances and data will not be disclosed.

2 Lens system breakdown & Boundary conditions

This chapter will describe the system and operating conditions. First the system layout will be explained, next the key requirements, followed by the boundary conditions and finally the open issues.

2.1 Lens system layout

The electrostatic lens consists of two circular silicon elements that are mounted on top of each other. The elements have a large potential difference (tens of kV) and are kept apart by an electrically insulating ring shaped spacer. The elements are solid silicon except for the beam area, which is perforated by a grid of holes. The top and side view can be seen in Figure 4.

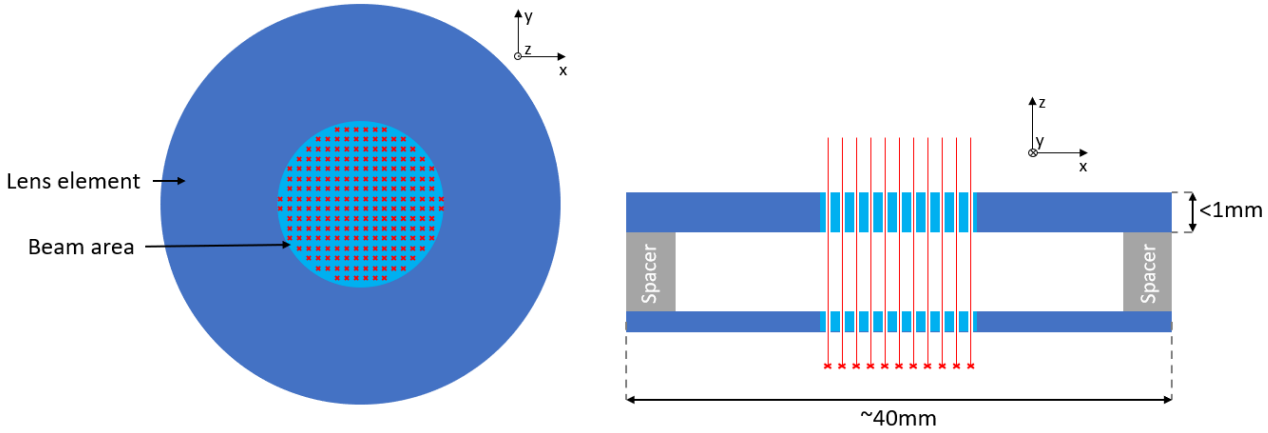

Figure 4: Schematic layout of the lens system (not to scale)

2.2 Key requirement

The objective of the project is defined as keeping the focal plane as flat as possible within a sub-micrometer budget. This error can be translated to the positions of the lens elements, lens geometry and potential difference between the lens elements. If the bottom lens element moves down, the focal plane will move down with the same distance. If the distance between the two elements becomes larger, the electric field strength will decrease. A weaker field decreases the lens strength, therefore moves the focal plane down. Using electron optics (which is out of scope for this report) the change in focal plane with respect to the bottom lens element is equal to $\frac{1}{2.4}$ of the change in distance between the lens elements. If we define downwards as positive, the above mentioned relations come down to equation 1 where δB and δT are the bottom and top element displacements respectively. Note that the lens displacement errors can be both positive and negative.

$$\delta FP = \delta B + \frac{1}{2.4} * (\delta B - \delta T) \tag{1}$$

Equation 1 holds for every beam, therefore the distance between the elements is relevant for the entire beam area.
For the electrostatic lens to work an electric field needs to be created between the two elements. This requires a potential difference between the elements which is in the order of a few tens of kV. This difference in potential creates electrostatic forces that will cause both elements to be attracted to each other, bending the elements inwards and changing the focal plane.

2.3 Boundary condition

Next to the vertical budget, there are also restrictions in the allowable horizontal errors. The holes of the top lens element should be aligned with the holes on the bottom lens element within a few micrometer. Due to this restriction the choice in bonding methods of the elements to the spacer is limited (this will be explained further in chapter 3). The bonding method will again have effect on the vertical errors.
Electron beams cannot travel through air, therefore the inside of the machine will be Ultra High Vacuum (UHV), in this field UHV is defined as a pressure below 10e-6 mbar. Some materials experience outgassing in these conditions, which is the effect of solid materials releasing gasses in very low pressures. When more out gassing components are present within the vacuum chamber a stronger pump is required to achieve the same vacuum. This problem occurs with most plastics and even some metal, these materials should be avoided in the design. Due to the UHV any heat has to be transferred by conduction (lens temperatures are <30°C, therefore radiation is negligible). If the cooling is not sufficient the temperature will increase, which will change the focal plane due to thermal expansion. The components that heat up are all located around the beam area. The effects and the resulting errors of these components will be discussed further in chapter 4.
There are also size limitations on the elements. The bottom element has a very small volume claim, therefore the thickness of this element is limited to a few hundred micrometer. The top element thickness is only constrained by the etching depth (we require through holes for the beams). Typically, to etch deep holes a Bosch etching process is used (see figure 31). This process can etch relatively deep holes by repeatedly etching the same hole while applying a passivation layer on the sides. A general rule of thumb for Bosch etching is that the depth can be up to ten times the feature size. Using this rule of thumb the top element is allowed to have about two times the thickness of the bottom element.
The diameter of the element is determined by the size of the beam area and some clearance between the beam and the spacer. When stray electrons land on the spacer it will gain a charge as the electrons cannot escape (the spacer is electrically insulating), the clearance must be large enough to prevent the electric field from the charged spacer to influence the electron beam. A rule of thumb for this effect is the 1:5 rule, meaning that the distance between the spacer and the beam must be 5 times large than the distance between the elements (see figure 5) The beam area and the clearance will result in an element with a minimum diameter of a few tens of millimeters.

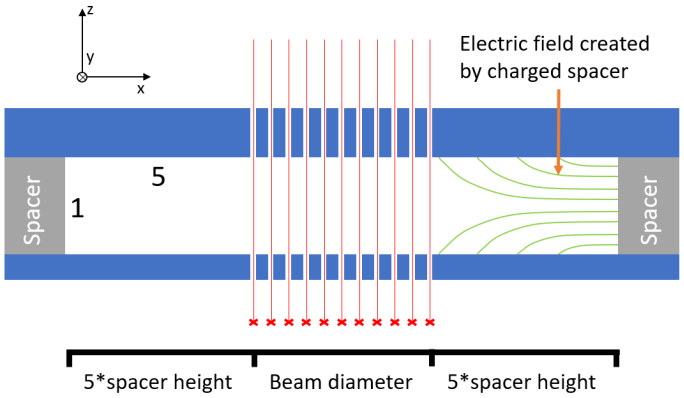

Figure 5: 1:5 rule (not to scale)

The basic design and material properties are largely determined by the lens design and electron optics, therefore the lens layout and materials have already been chosen and cannot be changed. The materials for the lens elements and spacer have to be silicon and borosilicate glass respectively. Silicon is chosen for its microfabrication capabilities, low CTE and thermal conductivity, borosilicate glass for its electrical insulation and comparable CTE to silicon.

2.4 Open issues

The objective, boundary conditions and some design choices are now clear, however, some open issues still remain. To prevent the scope of the project from becoming too large the focus will remain on the lens element stack (both lens elements and the spacer). As explained above the basic layout cannot be changed, however the bonding between elements and spacers has not yet been defined. The bonding of these elements will have a large effect on the flatness of the elements, therefore they will be discussed in the next chapter.

3 Design Choices

This chapter will cover the trade offs made for the open issues of chapter 2.4. In chapter 3.1 different bonding methods will be compared for connecting the lens elements and spacer, which will result in adhesive bonding being the most promising solution. Another trade-off follows in chapter 3.2 to determine the most suitable adhesive.

3.1 Bonding trade-off

First the requirements on which the bonding methods will be judged are explained, next the different bonding methods will be discussed.

3.1.1 Bonding requirements

The following requirements have been defined for the bonding between the lens elements and the spacer:

- **Shear strength**: The elements will be bonded with a high precision on the XYRz alignment. During handling, transport and mounting the bonding should not fail otherwise this precision will be lost. On top of that the electric field will cause the elements to bend inwards, which in turn will expose the bonding to a shear force. The expected shear stress on the bonding due to the electric field has been calculated using FEM and is in the order of 1 MPa, including a safety factor the shear strength should be higher than 3 MPa. During transport the difference in CTE between borosilicate and silicon will apply a shear force on the bonding. However, the force caused by the thermal expansion is lower than the 1 MPa applied be the electric field.
- **Stress free suspension**: The element will only be supported at the spacer edges, therefore stress inside the element can influence the flatness. In case of compressive forces the element can buckle and in case of tensile forces outside of the neutral line the element can also bend (see Figure 6). To achieve the highest flatness possible the element should contain as little stress as possible or tensional stress along the neutral line. A likely source of stress inside the elements is thermal expansion. The spacer material is selected on having a very comparable CTE to silicon, however small differences remain. The CTE of a material is not constant with temperature, when the temperatures changes, so does the CTE. In Figure 7 the CTE of silicon and Pyrex (a brand name for borosilicate glass) is plotted against the temperature. When the positive and negative surface between the lines is equal both materials have expanded the same amount from room temperature, meaning that if the material bonds at this temperature, the bond will be without stress at room temperature (which is the operation temperature for the lens stack). Therefore, this requirement comes down to either bonding at room temperature or around 440°C. If an element is bonded at 440°C the element will be stress free at room temperature. However, during the cooling down large amounts of stress occur. The largest shear stress that occurs during cooling down is about 1.5 times the requirement of the shear strength. Therefore if a bonding temperature of 440°C is used the shear requirement increases to 4.5 MPa.

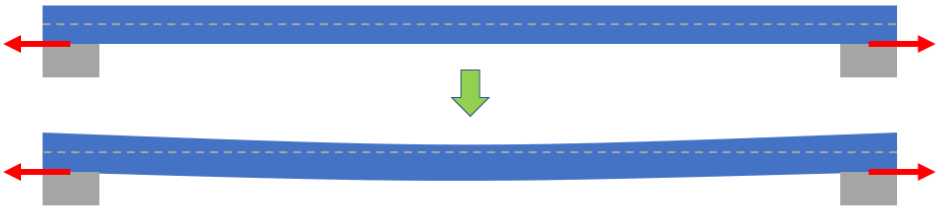

Figure 6: Element with tension outside of the neutral line

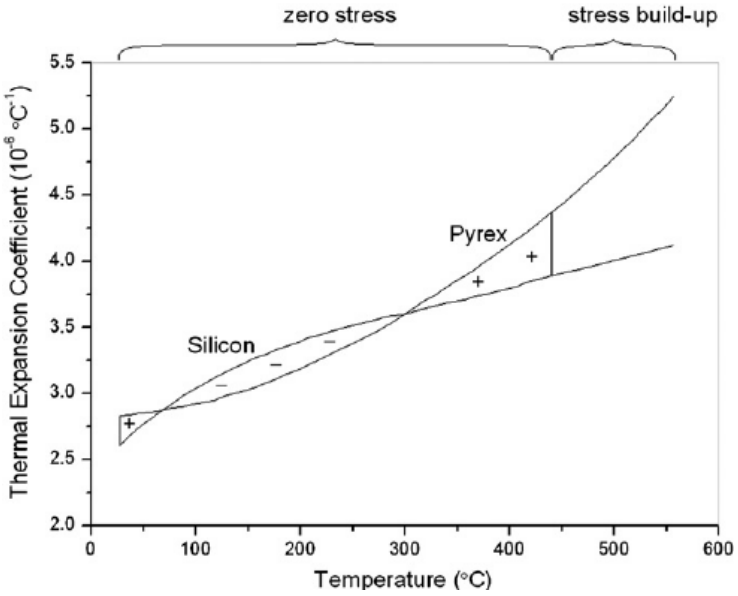

Figure 7: Stress free bonding range of Pyrex and silicon (note that Pyrex is a branded name for borosilicate glass) [9]

- **Particle sensitivity**: Some bonding methods can use fillers to bond materials together (e.g. adhesives and soldering). These fillers will surround any particle contamination on the surface up to the thickness of the bonding layer. Other methods require direct contact between the two surfaces. Hence, particles can ruin the bonding. These methods are therefore very sensitive and prone to failure if there is a mistake in the process. Methods that are less sensitive to particles are preferred.
- **XYRz alignment**: There are two requirements for which a precise XYRz alignment is necessary. First the hole grid of the top and bottom element need to precisely align. Therefore, the position error of both elements with respect to each other may not be larger than a few micrometer. Secondly the beam grid introduces a less rigid spot in the element. If this spot changes position due to misalignment the curvature will change too (see figure 8), causing a deviation in the height of the element. This requirement is defined by the position of an element relative to the spacer and is calculated using Comsol. In figure 9 the vertical error is plotted for a few misalignment values (unfortunately due to IP the units of these values cannot be disclosed), the plotted error caused by this effect can largely be compensated (more on this in chapter 4.3). To still have an acceptable flatness error the element to spacer alignment error can be significantly larger than the element to element error, therefore the element to element error will be limiting for this requirement.

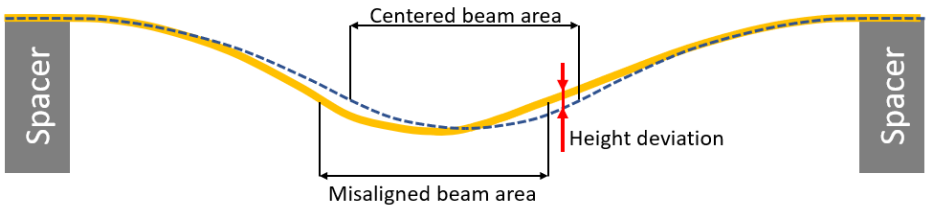

Figure 8: Schematic bending of a misaligned lens element and the caused height error

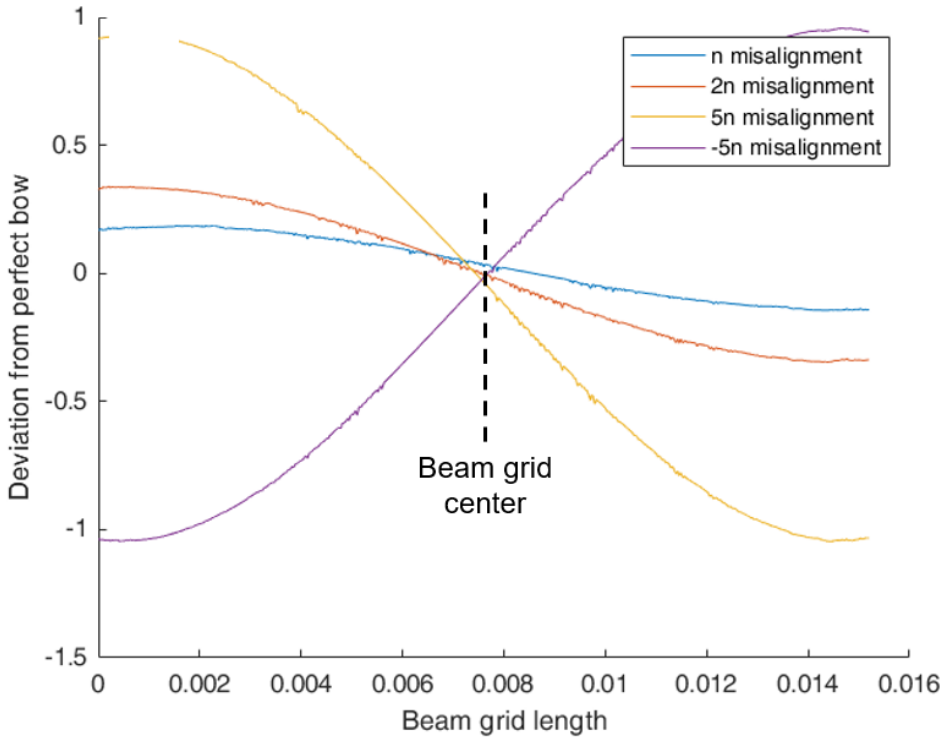

Figure 9: Change in flatness due to misalignment (units are removed for IP purposes)

To reach the required alignment precision stacking robots are used which operate at room temperature. The available stacking robots reach the highest precision if the elements can still be finely positioned after being brought into contact (this can be easily achieved with adhesives and beads), direct contact between two elements will create too much friction for fine positioning.
If the parts are moved or heated the alignment reached in the stacking tool may be lost. Therefore this requirement either limits the bonding temperature to room temperature or a heated stacking tool is required.

- **Survival temperature**: According to regular transport requirements a package can be exposed to temperatures from -25°C to 60°C. The CTE differences between silicon and borosilicate glass will create a shear load in the bonding, but the created load is still lower than the above mentioned strength requirement. The properties of a bonding method can change with temperature, which together with the thermal load might cause the bonding to fail. Therefore the bonding should be able to withstand these temperatures. However, if necessary, special transport requests can be made.

3.1.2 Bonding methods

There are many bonding methods that are able to bond silicon and glass together, the most promising methods are explained and compared below. Each of them will be judged for the requirements mentioned above.

- **Shrink fitting**: By working with differences in CTE an element can be shrink fitted to another. At the right temperature range the silicon wafer will shrink more than the borosilicate spacer, bonding the elements together. This method creates very strong bonds with a tensional load along the centre line. Downsides of this method are high loads, difficult alignment and tight machining tolerances.

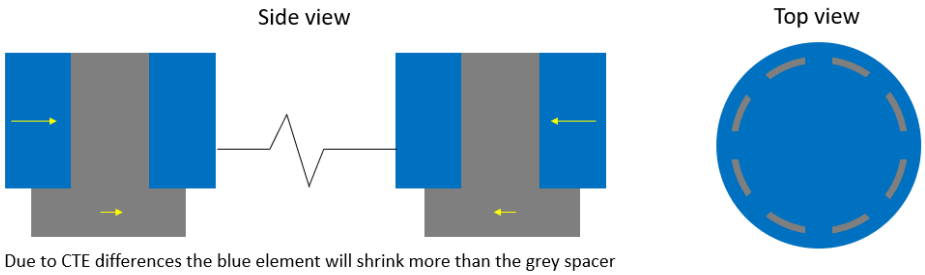

Figure 10: Schematic view of shrink fitting a lens element on the spacer

- **Adhesive bonding**: Adhesives are a widely used method of bonding due to high alignment precision and room temperature bonding (the adhesive can be cured at higher temperatures for improved performance). To prevent the operator from adding too much adhesive and to define the layer thickness, beads are mixed with the adhesive. The beads also act as rollers for the element to move on top of them, this allows for very fine positioning. However, if adhesives are cured at room temperature they often have a low glass transition temperature, meaning that the adhesive loses its strength at higher temperatures (see figure 11). If the stack reaches a high temperature during transport the load on the bonding will become larger (due to the CTE difference) and the adhesive will lose its strength. If the increased load is larger than the strength of the weakened adhesive the elements can move and lose their alignment. On top of that the adhesive might reattach in the warmer state, applying a load when cooled down which can potentially move the focal plane out of focus. Next to the low temperature resistance adhesives tend to drift due to viscoelastic creep, shrink when curing and exhibit hygroscopic swelling.

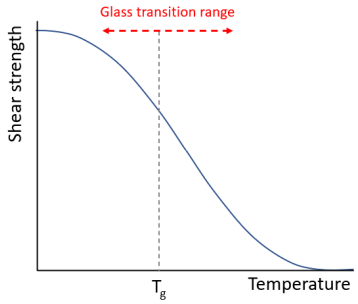

Figure 11: Glass transition temperature of adhesives

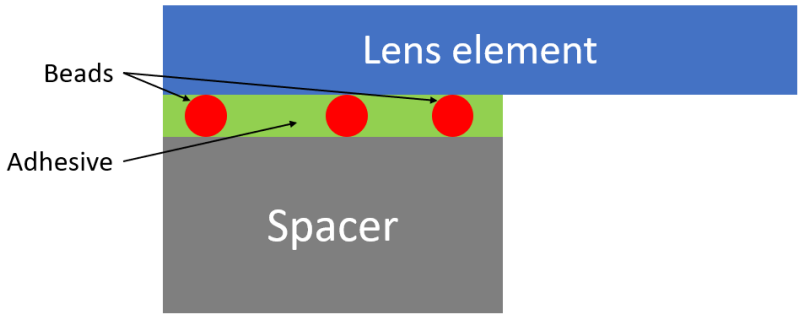

Figure 12: Defined adhesive layer thickness with beads

- **Glass frit bonding**: By solidifying a layer of molten glass between two elements they can be bonded together. This method creates very strong bonds, but it requires minimal temperatures of 450°C. This temperature is above the bonding range for borosilicate glass and silicon (see Figure 7), therefore the bonding will not be without stress at room temperature. Additionally the bonding layer is very stiff, exposing the elements to high forces when cooling down. As the bonding happens at high temperatures alignment will be a big issue.

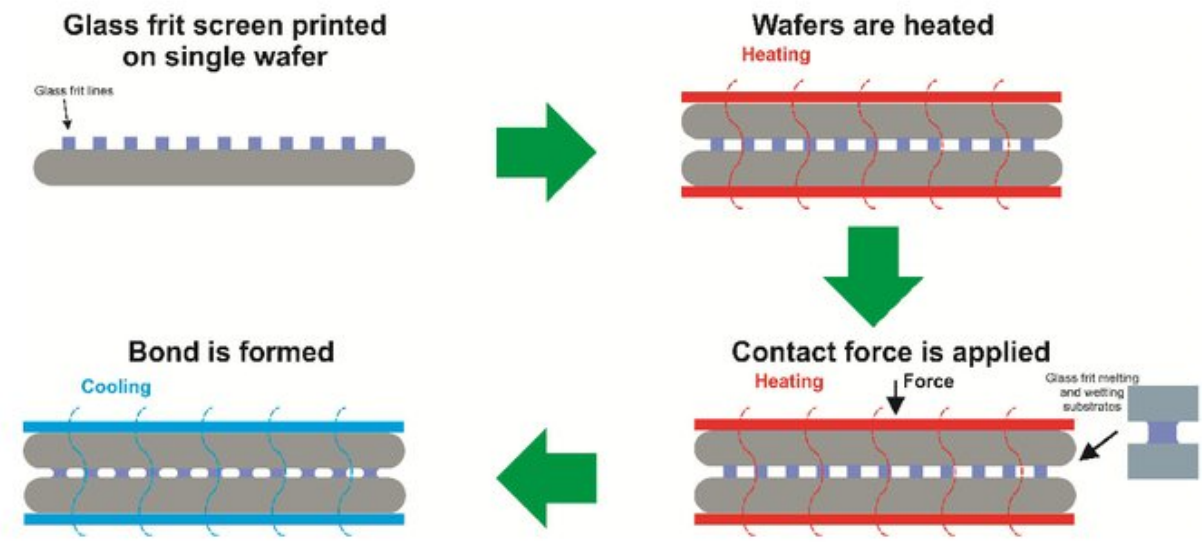

Figure 13: Process steps for glass frit bonding [3]

- **Anodic bonding**: Anodic bonding is a method that is often used between borosilicate glasses and silicon. By applying a large potential difference between the two elements mobile ions are pulled to each side. This leaves Si+ and O2- at the contact surface of silicon and borosilicate glass respectively. At temperatures of 400°C the silicon and oxide-ions will form siliconoxide, bonding the elements together. This method creates very strong bonds, however due to the high temperature, alignment is again a major issue. On the positive side the bonding can be created at the stress free bonding range, however due to the high bonding stiffness the material will be exposed to high loads when cooling down. Another problem with this method is that it can only be applied to one side, as exposing a bonding to a reversed potential (which is necessary to bond the other side) will destroy the bonding. However this problem can be circumvented by combining different bonding methods.

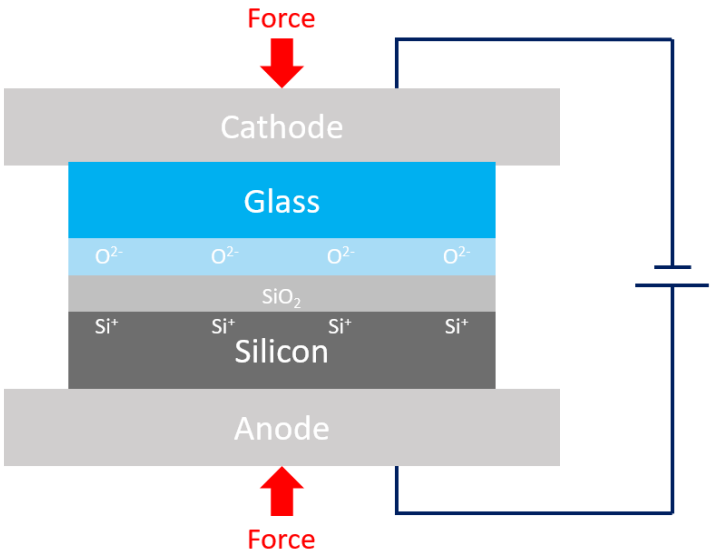

Figure 14: Schematic overview of anodic bonding

- **Optical contacting**: This method creates a bond of reasonable strength using van der Waals forces and covalent bonds (1MPa van der Waal, 5 MPa covalent). Covalent bond require a silicon silicon bonding, but this can be reached by depositing a silicon layer on the spacer. This should result in a bonding strength of about 6MPa, however, in practice the result is often lower (∼4MPa). This bonding method can be created at room temperature, however it is prone to failure (one particle can ruin the bond) and it is very sensitive to CTE differences (a small increase in temperature can break the bond). Although the bonding can be created at room temperature, during transport the CTE sensitivity can still become a problem.
- **Direct bonding**: Direct bonding uses pure heat to bond two silicon elements together (therefore a silicon layer has to be deposited on the spacer). At temperatures above 200°C OH groups in the silicon surface will react creating Si-O-Si bonds and H_2O. At temperatures above 950°C the H_2O will break down creating additional oxygen for Si-O-Si bonds, the remaining hydrogen will diffuse through the wafer leaving a strong bond without air pockets. This bonding technique requires high temperatures and cannot bond at the CTE bonding range. On top of that it is very sensitive to CTE differences.

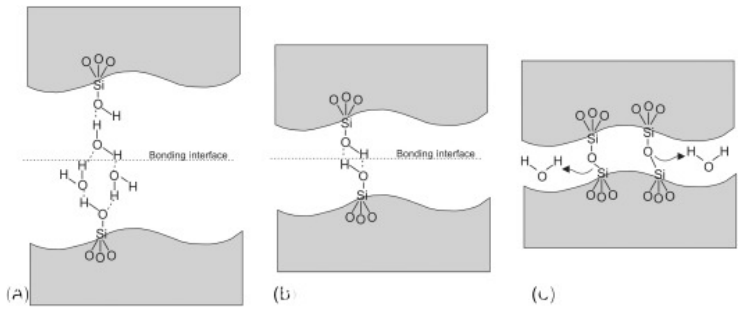

Figure 15: Silicon oxide bonds created with direct bonding [10]

- **Surface activated bonding**: By bombarding the surface with Argon atoms in UHV the surface is atomically cleaned, meaning that adsorbed contaminants and native oxides are removed from the surface. If two of these activated surfaces come into contact with each other they will directly bond, these bonds have shown a shear strength of up to 10 MPa [12]. Argon plasma will deeply clean the surface of the materials, however it will not remove particles. Therefore this method is also very sensitive to contamination. The materials are bonded to each other without a filler, therefore this method is also very sensitive to CTE differences.

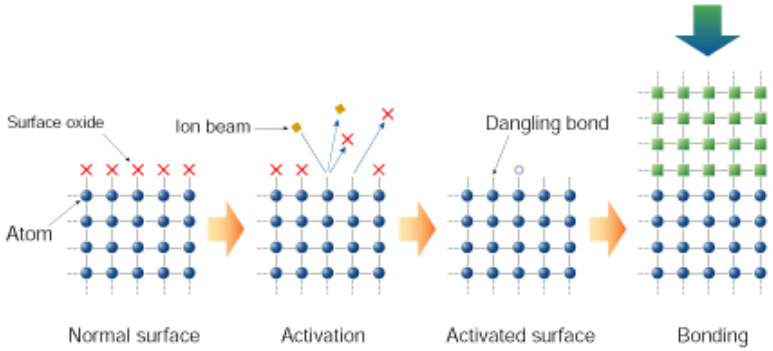

Figure 16: Surface activated bonding steps [12]

- **Eutectic bonding**: two elements can be bonded together by solidifying a layer of molten metal in between them (e.g. soldering). By combining two metals into an alloy a melting temperature can be reached that is lower than either of the original metals, this is called an eutectic system. The lowest melting temperature can be achieve with gold and indium at 157°C [7], however by using the correct metals and ratio's nearly every temperature can be reached. This allows for bonding at the stress free bonding range to reach a stress free suspension.

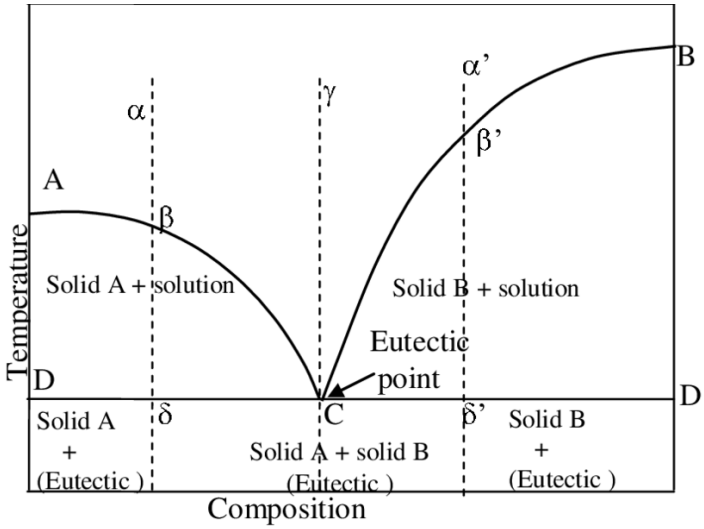

Figure 17: Eutectic system melting point [8]

3.1.3 Bonding trade-off

Each of the above mentioned methods will be judged on the requirements in table 1. When a cell is green the method satisfies the requirement, when it is orange the requirement will be a challenge and when it is red the requirement is either too difficult or not feasible at all. Therefore if a bonding method contains a red cell it will be dropped.

Method	Shear strength [MPa]	Temperature [°C]	Particle sensitivity	Alignment	Survival temperature [°C]	Remarks
Shrink fit	>50	>100, but center-line tension	Little	High machining tolerances	>60	Alignment issues, high machining tolerances
Adhesive bonding	~10	RT	Filler, not sensitive	RT and easy adjustment	Depends on adhesive, typically >40	Very easy to apply, high tolerances, susceptible to drift and other unpredictable effects.
Glass frit bonding	~25	>450	Filler, not sensitive	High bonding temperature	>60	Sensitive to CTE differences
Anodic bonding	~20	200-500	Sensitive	High bonding temperature	>60	Difficult to apply on two sides of a part, requires split spacer, sensitive to CTE differences
Optical contacting	~4 (extremely sensitive)	RT	Very sensitive	RT, but no movement after touchdown	>60	Requires very flat and clean surfaces, not very strong, very sensitive to contaminants and CTE differences
Direct bonding	~25	200 and 950	Sensitive	High bonding temperature	>60	Requires very flat and clean surfaces, little control over bonding temperature, sensitive to CTE differences
Surface Activated bonding	~10	RT	Very sensitive	RT, but no movement after touchdown	>60	Requires very high cleanliness, sensitive to CTE differences, rare technique with very few manufacturers
Eutectic bonding	>25	160-450	Filler, not sensitive	High bonding temperature	>60	Requires rare combination of metals, very long lead times

Table 1: Bonding trade-off: Green cells meet the requirement, orange cells are a challenge, red cells do not meet the requirements

The bonding methods below are dropped because of the following reasons:

- Shrink fit: The alignment requires machining tolerances that are not realistic (sub 5 micrometer).
- Glass frit bonding: Requires a bonding temperature outside of the stress free bonding range, this will cause too much stress inside the element.
- Optical contacting: Bonding strength is unreliable, a single particle can destroy the bonding.
- Direct bonding: Bonds outside the stress free bonding range, therefore it will cause too much stress inside the element.
- Surface activated bonding: The method looks very promising, however this method is very complicated and mostly used in experimental settings (almost no manufacturers offer this service). On top of that this method is also very sensitive to contaminants.
- Eutectic bonding: Requires a rare combination of metals, it will take a long time to find a manufacturer that is able to comply to the very specific demands. On top of that even if a manufacturer is found the lead times will likely be very long.

This leaves 2 methods which will be further investigated, adhesive and anodic bonding. Adhesive bonding has the benefit of room temperature bonding, good alignment and easy application, the downsides are low temperature resistance and various other effects like drift, shrink and hygroscopic swelling, of these effects especially drift is not desirable as a small amount of drift can result in a large vertical displacement. Anodic bonding is strong and stable, however it requires high temperatures and is difficult to align. On top of that it can only be applied to one side.
To circumvent the problem of only being able to anodically bond one side a combination of both methods is considered; the bottom element is anodically bonded while the top element is glued. As mentioned in section 2, the top element is significantly thicker than the bottom element. Therefore the bottom element will bend more and apply a larger shear force on the bonding than the top element. By only gluing the top element large shear forces in the adhesive are avoided, minimizing the effect of drift.
The alignment requirement consists of two sub requirements, one defines the tolerance from element to spacer and the other from element to element (the latter is more strict). The element that is bonded first has to comply to the first requirement, while the second element that is bonded has to comply to the more strict second requirement. By anodically bonding the bottom element first and gluing the top element second the very tight alignment problem can be circumvented (see figure 18).

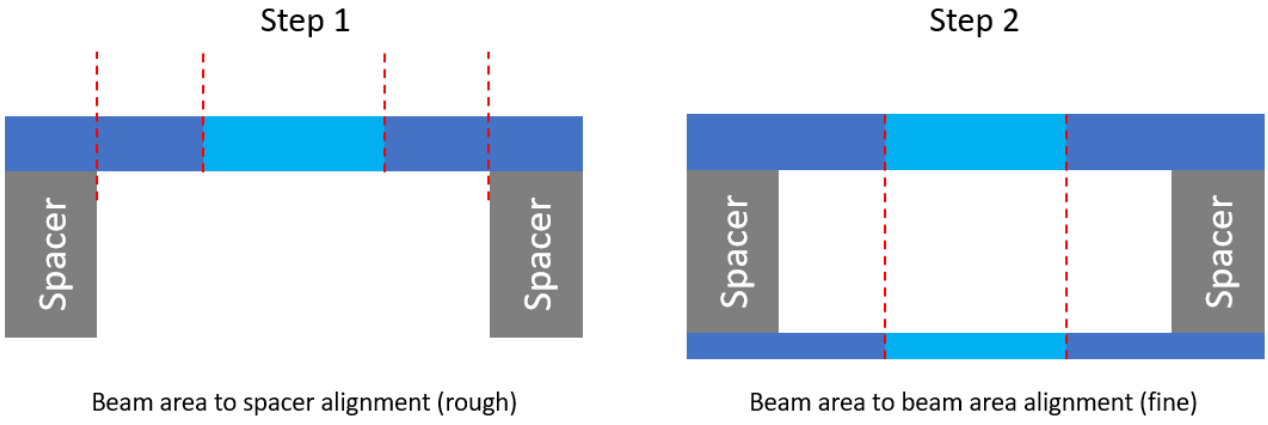

Figure 18: Alignment steps, the positioning requirement on the first element is less strict than the second

Although it is possible to reach the alignment requirements using this method a few problems remain. The top element is still relatively thin, due to the large thermal stresses when cooling down the element has a large risk of shattering. On top of that anodic bonding usually requires a few iterations to optimize the process, it is not feasible to have a lot of iterations in the time span set for this project. Therefore adhesive bonding is chosen for attaching both lens elements to the spacer.

3.2 Adhesive trade-off

3.2.1 Adhesive requirements

The properties of adhesive bonding strongly depend on the used adhesive. Therefore a proper adhesive has to be selected. Using the databases of both ASML and Mapper multiple adhesives are selected that are able to bond to both metals (silicon) and glass (borosilicate glass) and can be used in vacuum. The remaining requirements are the same as for the bonding trade-off, although they are now redefined in properties of the adhesives (e.g. alignment becomes viscosity). The adhesives will be judged for the following requirements:

- **Strength:** As described in the previous strength requirement the calculated shear stress in the bonding is at most 1 MPa, including a safety factor any value above 3MPa will be fine.
- **Bonding temperature:** The CTE of the spacer and element are close but not the same, to achieve stress free suspension and the best alignment results (close to) room temperature bonding is required. Potentially the adhesive can also be cured in two steps. First the adhesive is partially cured at room temperature to lock the position, then a secondary higher temperature cure is applied while the original curing hold the elements in place.
- **Viscosity:** In a stacking robot the precise alignment is actuated after the element makes contact with the spacer. Adhesives with lower viscosity have more resistance when placed and during compression, this decreases the stacking robot precision and can potentially leave residual stresses which are not desirable.
- **Survival temperature:** The bonding needs to withstand the shear forces created by the differences in CTE and transport temperatures. Although the exerted shear forces are lower than the strength requirement, additional temperature effects on the adhesive can be a problem. When adhesives cool down they become more brittle. Combined with the increased shear forces this could potentially cause a brittle fracture. When adhesives heat up they reach their glass transition temperature. Around this temperature the adhesive will slowly lose its strength and the modulus of elasticity will decrease. The glass transition temperature (or Tg) depends on the adhesive and the curing process; generally lower curing temperatures result in a lower Tg. As a low bonding temperature is required for stress free suspension this requirement will be difficult to satisfy.
  Most adhesives have more issues with high than low temperatures and on top of that high temperatures are more likely to be encountered. Therefore, this requirement will focus on the maximum temperature resistance of adhesives. However, keep in mind that special request can be made for transport making this requirement optional.

3.2.2 Adhesive trade-off

The adhesives are judged for the requirements using the same colour scheme as before. Green indicates that the adhesive satisfies the requirement, orange that it is on the border but can be worked with and red indicates that the adhesive does not satisfy the requirement. The strength requirement will be skipped as all adhesives easily satisfy this requirement. Some of the properties of the adhesives can be improved with a higher temperature cure, but for this trade-off only the lowest advised curing is evaluated. Unfortunately for IP purposes the names of the adhesives may not be disclosed, therefore the adhesives will be named glue 1, glue 2 etc.

Adhesive	Lowest Curing T [°C]	Tg [°C]	Viscosity [Pa*s] (H2O=0.00089)	Remarks
ASML glue 1	RT	50	0.225-0.425	Often used, lot of experience
ASML glue 2	RT	49	15-25	Often used, lot of experience
ASML glue 3	RT	70?*	0.400	Small manufacturer, incomplete datasheet. Lot of experience
ASML glue 4	80	90	9-18	Often used, lot of experience
ASML glue 5	80	125-150	3-5	
ASML glue 6	80	100	25-40	
ASML glue 7	RT	60-75	75-250	
ASML glue 8	RT	40	0.150	Difficult adhesive to cure, Mapper switched to glue 3
ASML glue 9	RT	95	40	CMR adhesive (carcinogenic), difficult to use, recommended to avoid
ASML glue 10	RT	60	30	ASML recommends for repair use only

*The Tg is not specified on the datasheet, this value was estimated by one of the manufacturers technicians

Table 2: Adhesive trade-off: Green cells satisfy the requirements, orange cells are a challenge and red cells do not meet the requirements

There is not a clear preference for the choice of adhesive, for now the best three are selected. The adhesives below are dropped because of the following reasons:

- Glue 4, 5 & 6 all require a minimum curing temperature of 80°C, this is too high for stress free bonding.
- Glue 7 is too viscous, this will inhibit precise alignment.
- Glue 8 was often used by Mapper, however the quality of the curing changed from operator to operator. Therefore Mapper switched to glue 3.
- Glue 9 has been identified as a CMR chemical (Carcinogenic, mutagenic or toxic to reproduction, in this case the adhesive is cancerous).
- Glue 1, 2, 3 & 10 are all good options. In the next chapter it will be explained that adhesives have some difficult to predict properties and will therefore be tested in experiments. To limit the amount of tests necessary only 3 adhesives are selected. Therefore glue 10 is dropped. Glue 1, 2 & 3 are used a lot within ASML/Mapper, these adhesives are proven to be very effective and more research into these adhesives will be beneficial for both this report and ASML.

Glue 1, 2 & 3 have been selected as the best adhesives for this project.

4 Error contribution estimation

The focus budget of the SEM is shared with multiple components inside the machine. The lens elements themselves, lens stack position, wafer position and many more factors will influence the total budget. Some components will require a part of the total budget while other components can be used to compensate errors. In this chapter different error categories are explained and how they can be compensated, next the causes of errors are listed and categorized in the previously mentioned categories and finally the size of each error is estimated.

4.1 Error categories and compensation

The error budget of the focal plane is very tight, therefore even the smallest errors in the lens elements or components near the lens will have a large effect on the focal plane budget. To loosen the tolerances multiple mechanisms are designed to compensate different kinds of errors, the following four error categories are considered, they are ordered by decreasing budget.

4.1.1 Vertical and tilt errors

If the lens stack is placed at the wrong height or the spacer is the wrong thickness a vertical error is created, the entire focal plane will either be too high or too low. These errors can however be easily compensated by moving the wafer, see figure 19. By adjusting the wafer any error where the focal plane remains flat (height and tilt) can be compensated, however, errors where the focal plane changes shape (like a bow error) can not be compensated using this method. The wafer has a relatively large range of adjustment and largely depends on lens placement (which is not within scope for this report), therefore this budget will not be covered in detail.

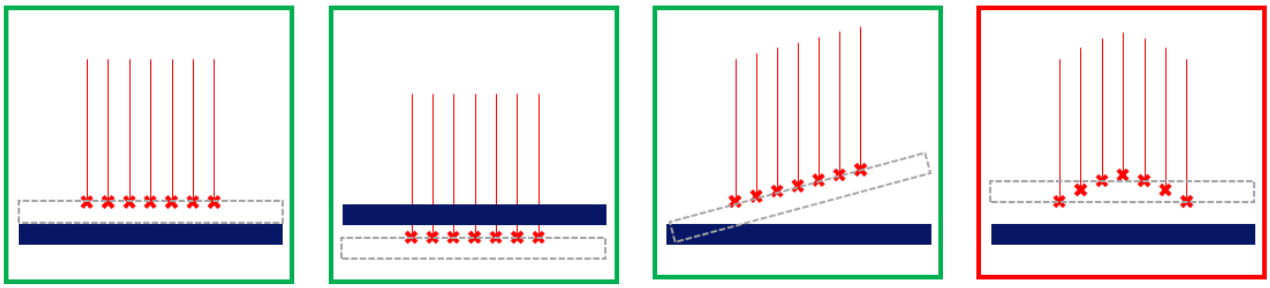

Figure 19: Error compensation by wafer repositioning

4.1.2 Systematic bow errors

The two lens elements have a large potential difference which will cause them to attract each other (see figure 20). These forces cause the elements to bend, bringing them closer to each other which increases the electric field strength. The variation in electric field strength together with the bend bottom lens element will cause the focal plane to curve. The potential difference and element stiffness is relatively well known (the systematic error is about 10 times the random error), therefore a good approximation can be made on the size of the bow. By adjusting the geometry of the lens elements the bow can be compensated. Adjusting the lens elements can only happen during production, therefore only the systematic bow errors can be compensated with this method.

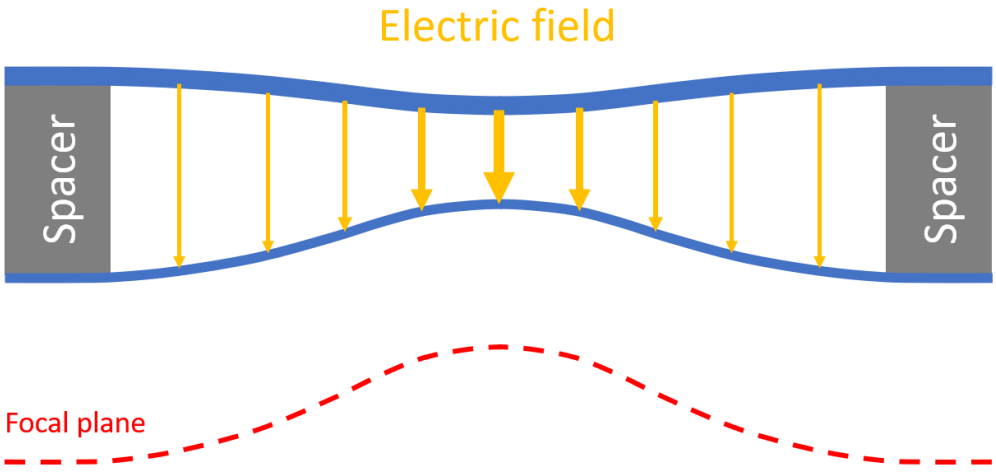

Figure 20: Bending of the focal plane due to potential difference between lens elements

4.1.3 Random bow errors

This category covers the random errors introduced with the systematic bow errors of the previous category (therefore this category is still axisymmetric). The systematic bending is determined by numerous parameters (which will be explained in chapter 4.2), each of these parameters has a tolerance which will cause a random bow error (which is an axisymmetric variation of the systematic bow error). The force that attracts the elements is caused by the potential difference. To compensate for some of the random bow errors this potential can be slightly varied. Changing the potential changes the bow of the element, which allows adjustment for random bow errors after production. the range of adjustment is less than a tenth of the range for systematic bow errors.

4.1.4 Non axisymmetric errors

Not every error will create a perfect bow error that can be compensated by adjusting the potential. For example, if the beam grid location is not located in the centre of the spacer (the XYRz alignment mentioned in chapter 3) a non axisymmetric error is created. Although some of the created error can still be compensated by adjusting the bow and tilt a large part of this error can not be compensated.

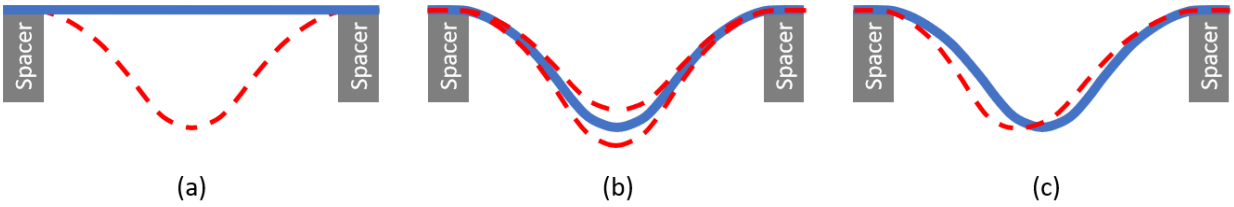

Figure 21: (a) systematic bow error, (b) random bow error, (c) non axisymmetric error

4.2 Expected error contributions

The errors are subdivided in categories based on their shape. Each category has a budget, the size of the budget is determined by how much can be compensated with the previously explained compensation methods. This sub-chapter will focus on which parameters can cause focal plane flatness errors. For each category the expected error sources and parameters will be explained. The vertical and tilt error budget is largely dominated by the placement tolerances of the lens stack and wafer (see figure 22) which is out of scope for this report. On top of that this category does not create a focal plane flatness error, it only changes the position of the plane, not the flatness. Therefore, as this report is focused on the focal plane flatness errors, the vertical and tilt error category can be dropped. However, this category can still be used to partly compensate non axisymmetric errors, which will be explained later.

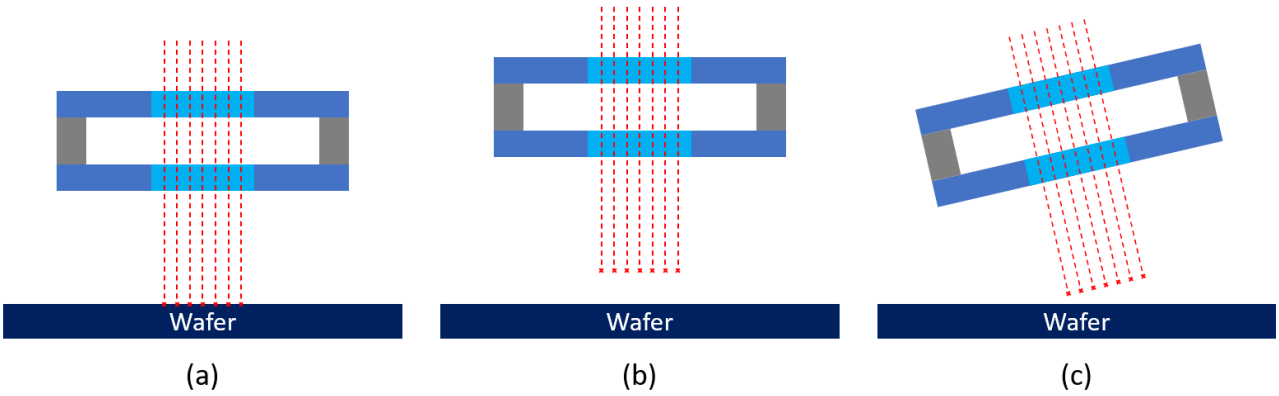

Figure 22: (a) correctly placed lens stack, (b) vertical error on lens stack placement, (c) tilt error on lens stack placement

4.2.1 Systematic bow error

The ideal lens element would be perfectly flat, therefore any disturbance that causes the elements to systematically deflect from its flat state is a systematic bow error. The equation for the deflection of a circular clamped plate under a uniformly distributed load can be seen in equation 2a [4], where δ is the deflection in m, p the pressure in Pa, r_0 the plate radius in m and D the bending rigidity defined as equation 2b (where E is the Youngs modulus in Pa, t the plate thickness in m and ν the Poisson ratio).

$$\delta = \frac{p r_0^4}{64D}\left[1 - \frac{r}{r_0}^2\right]^2 \qquad (2a) \qquad\qquad D = \frac{Et^3}{12(1-v^2)} \qquad (2b)$$

Every parameter in these two formula's will contribute to the systematic bow error. The pressure, radius, Youngs modulus and Poisson ratio are all defined as explained in section 2.3. The only remaining parameter is the thickness, which should be maximized within the volume budget to minimize the amount of bending. Four factors that are not covered in the basic formula are the hole grid in the beam area, the pre-existing bow, thermal expansion and bonding effects. The grid of holes will weaken the bending rigidity and increase the amount of bending in the lens elements, the pre-existing bow will add (or subtract) to the deformation caused by the potential difference, thermal radiation from nearby components will cause the elements to heat up and expand and bonding effects like elasticity and drift can allow an element to sag.

4.2.2 Random bow error

The random bow errors depend on the tolerances of the parameters mentioned above and a few additional ones. The pressure p, radius r_0 and the thickness t depend on the used electronics and the manufacturing process and will therefore have a tolerance. The Youngs modulus E and the Poisson ratio ν are material constants and are therefore assumed as constant. The Youngs modulus does however change with temperature, but as the temperature of the elements is relatively stable (remains between 20 and 30°C) this effect is negligible. Therefore, only the following parameters are considered to contribute to the random bow error:

- **Force:** The size of the distributed force is determined by the difference in potential between the lens elements and the distance between them. The tolerance on the potential difference is determined by the electronics controlling them, the tolerance on the thickness by the spacer and bonding thickness tolerances.
- **Radius:** The error on the radius is determined by the inner diameter of the support, which will be determined by the production tolerances of the spacer.
- **Element thickness:** The element thickness determines the bending rigidity with the power of three, therefore small differences in thickness will have a large effect on the random bow errors. This value will be one of the largest contributors the this error category.

Next to the tolerances on the parameters of the bending equations 2a and 2b there are some additional values that will influence this error category:

- **hole size & taper:** As mentioned in the systematic bow errors section, the grid of holes will influence the bending rigidity of the elements. The shape of the holes (hole diameter, taper, ellipticity and pitch) will determine how much rigidity is lost. These factors will have a defined tolerance, which will determine the effect on the random bow error.
- **Wafer bow:** No wafer is perfectly flat, they are usually provided with a tolerance on the pre-existing wafer bow. When the elements are bonded to the spacer they are flattened on a vacuum chuck. When the element is released from the chuck it will try to return to its original position. If a rigid bonding method is used this might be prevented and will introduce residual tension instead. However, adhesives will most likely allow to element to return to its original shape with a bow. Therefore, this tolerance will directly add to the random bow error.
- **Thermal expansion:** There are some active components near the lens elements which will generate heat. These components will radiate heat to the lens elements causing them to heat and expand. The temperature will reach a steady state inside the lens elements (which causes a systematic error), however there is also a certain temperature stability on the steady state which will cause a random error.
- **Element bonding:** The elements will have to be attached to the spacer. The method of bonding has been determined in chapter 3 as adhesive bonding. Adhesives are prone to drift, shrink and hygroscopic swelling which can all cause random errors. These drawbacks strongly depend on the type of glue. Therefore, we can minimize these effects. And whatever is left is unfortunately difficult to model. As the glue is axisymmetrically applied the caused error should be a bow error, however as adhesives are difficult to apply and predict this might also cause some non axisymmetric errors.

4.2.3 Non axisymmetric error

The non axisymmetric error cannot be compensated and therefore has the smallest budget. The following errors are expected:

- **Non axisymmetric thickness:** The wafer manufacturer will provide a tolerance on the thickness which will indicate the total thickness of the wafer. Additionally it will also provide a TTV (Total Thickness Variation) which indicates the change in thickness within a wafer (see figure 23). The thickness and its tolerance indicate what the maximum and minimum values of the thickness could be, while the TTV indicates what the change in thickness within a wafer can be. For example, a 600± 10 μm wafer with a TTV of 2 μm can have a thickness between 590 and 610 μm, while the thickness variation within a wafer is smaller than $2\mu m$. If the thickness is not axisymmetric the element will not bend in a perfect bow, therefore the error caused by this effect will not be axisymmetric.

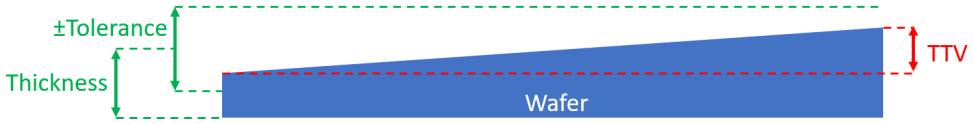

Figure 23: Difference between thickness and TTV

- **Beam area misalignment:** This error has been described in the XYRz alignment requirement in chapter 3. When the less rigid spot in the lens element (that is caused by the hole grid in the beam area) is moved with respect to the spacer, the bow of the element changes. This change causes a non axisymmetric error.
- **Element bonding:** As mentioned above the bonding is created with an adhesive, which are prone to many effects that are difficult to predict. On top of that the adhesive deposition will not be perfectly axisymmetric, which can cause non axisymmetric stress and thus deformation.
- **Spacer flatness:** The distributed force caused by the electric field is inversely proportional to the distance between the elements squared. Therefore, if one element is not perfectly parallel to the other the distributed force on the elements will change and cause non axisymmetric bending (see figure 24).

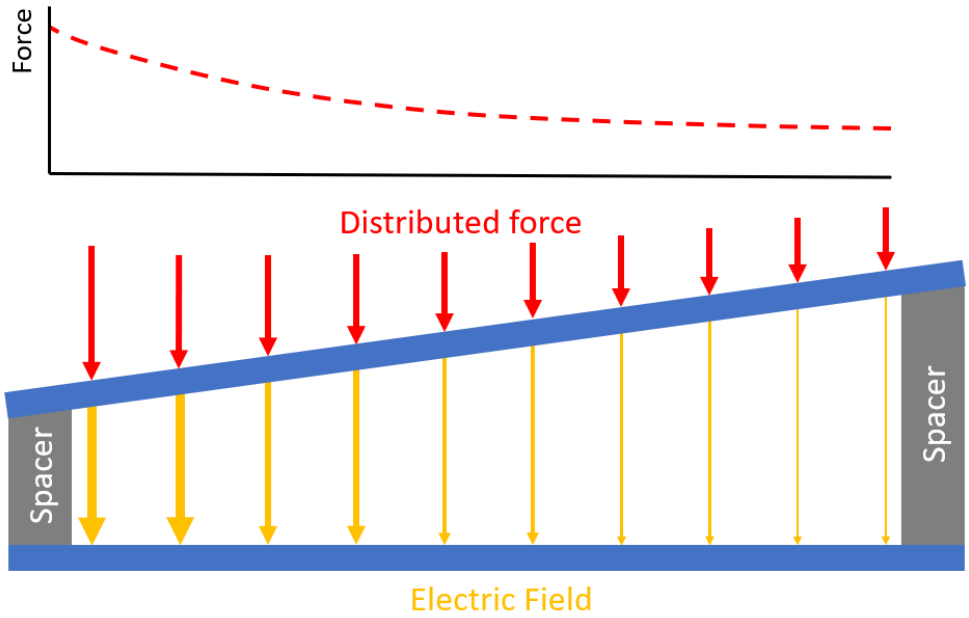

Figure 24: Non parallel elements result in a non linear force on the elements

4.3 Quantitative error estimates

To calculate the error budgets a quantitative estimate of each of the above mentioned errors is made. These estimates will show which errors are the most critical and should be focused on. The errors will be calculated using Comsol, a FEM programming which supports multiphysics. This allows different physics packages to be combined in a single FEM calculation. Where necessary, electrical mechanical forces, mechanical stiffness, heat transfer and thermal expansion can all be combined in a single calculation.

4.3.1 Model setup

To efficiently model the lens element a few simplifications are required. A single lens element is a thin circular silicon element, which is relatively easy to simulate with FEM. However, the beam area in the elements is a grid of holes. There are too many holes to efficiently simulate, therefore the grid of holes has to be simplified. There are two factors which will be influenced by the holegrid, the thermal conductivity inside the element and the bending rigidity. The holes can be simplified by approaching the element as solid but changing the values of these factors for an (decreased) effective value.
There are simple equations to approximate the effective thermal conductivity of a perforated plate, one of those can be found in equation 3a & 3b [6]. This equation is a good approximation for any parameters that linearly scales with the surface area. In this equation η represents the fracture of the remaining thermal conductivity, D the diameter of the holes and *density* the amount of holes per square meter.

$$\eta = \frac{1 - density * \pi * \left(\frac{D}{2}\right)^2}{1 + density * \pi * \left(\frac{D}{2}\right)^2} \tag{3a}$$

$$density = \frac{\#holes}{L * W} \tag{3b}$$

By multiplying the thermal conductivity of silicon with η the effective thermal conductivity is calculated, which can be used in the perforated beam area.
To validate the equation a small FEM model is build to test the thermal conductivity of a perforated plate (see figure 25). In this model a perforated and solid plate (for reference) are both exposed to a certain heatflux at the bottom and a fixed temperature at the top. Based on the maximum temperature reached at the bottom the thermal conductivity can be calculated. The result of the FEM model was within a few percent of the equation, therefore it is assumed that the equations are valid.

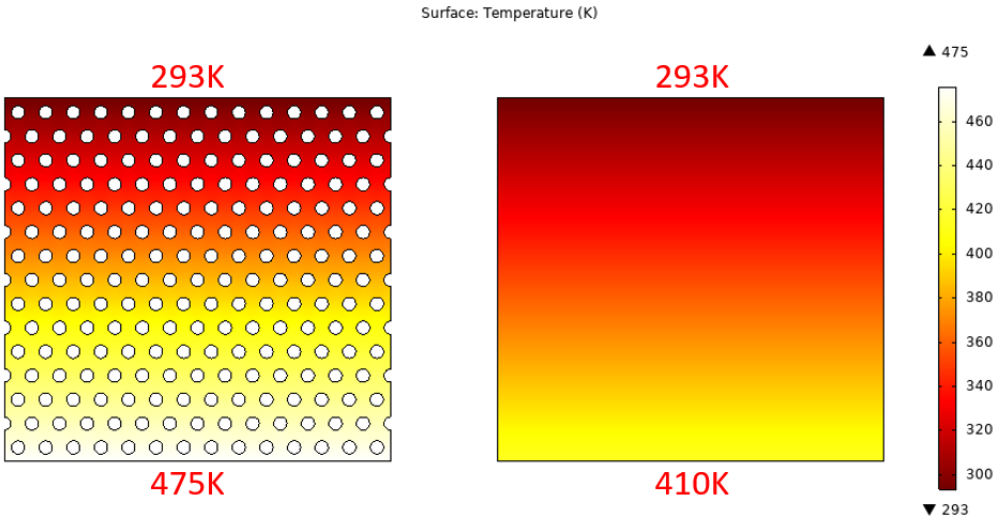

Figure 25: Effective thermal conductivity model used to validate the equation (not to scale)

The same method is used to calculate the effective Youngs modulus of a perforated plate. A perforated and solid plate are both exposed to a tensional load and by evaluating the displacement an effective Youngs modulus can be calculated.
The grid is however not isotropic. When heat travels through the sample it can take a shorter route in the horizontal direction than the vertical direction. The same isotropic behaviour holds for the effective Youngs modulus, when the sample is tensioned vertically there is not straight line of material to take the load. However, if the material is tensioned horizontally or at a 60 degree angle there is a straight line of material to take the load (see figure 26). Therefore the material will have a different Youngs modulus and thermal conductivity for different directions. To not over complicate the model and as the differences are not excessively large (about 5%) the effective thermal conductivity and Youngs modulus are averaged between their vertical and larger horizontal value.

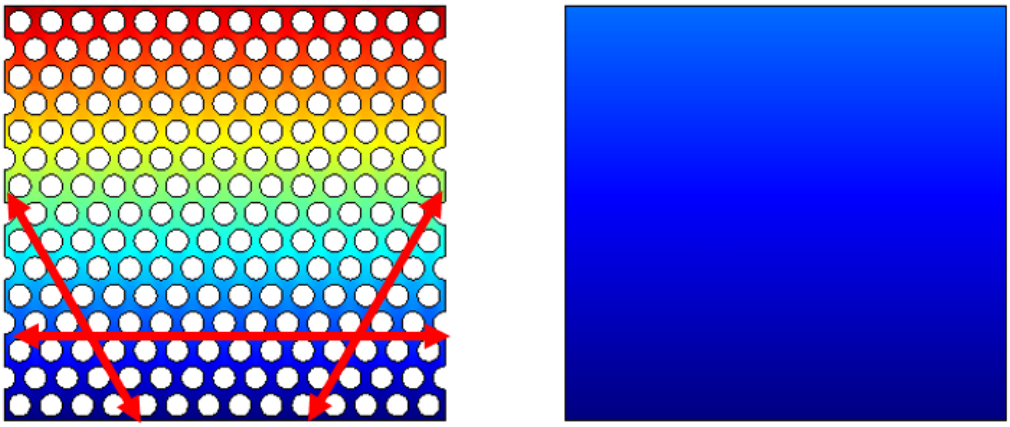

Figure 26: Anisotropic directions of a perforated plate (not to scale)

The effective thermal conductivity equation 3a for perforated plates yields the factor of the remaining thermal conductivity, in order to calculate the actual value this factor needs to be multiplied with the thermal conductivity of silicon. This value is often approached as a single number (often $130 W m^{-1} K^{-1}$), however, this value is not a constant. As the temperature changes the thermal conductivity will change too (see figure 27). In the operation range of the silicon components the thermal conductivity shows roughly linear behaviour, therefore it can be linearised in this domain with minimal error. The linearisation for the temperature range of 0 to 100 °C yields equation 4 (with T in Kelvin and λ in $W m^{-1} K^{-1}$).

$$\lambda = 315 - 0.556T \tag{4}$$

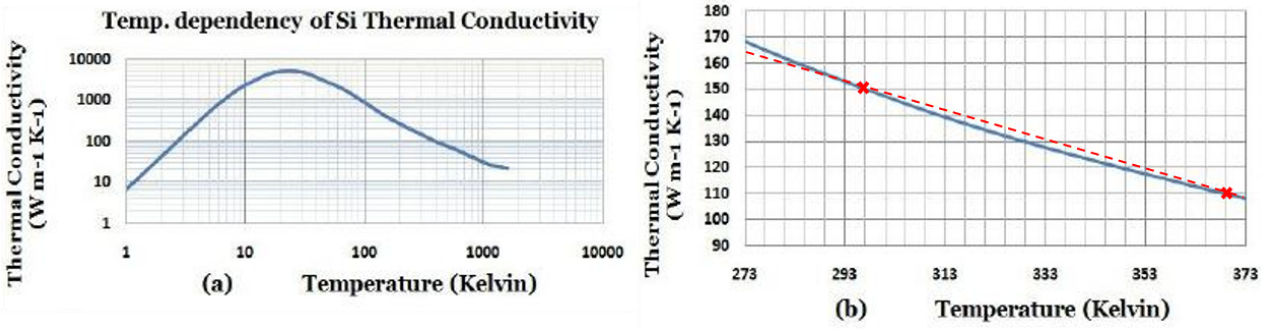

Figure 27: Temperature dependence of the coefficient of thermal conductivity [14]

The effect of a temperature dependant thermal conductivity will have little to no effect on the lens elements themselves (as they stay within a temperature range of 20 to 30°C). However this effect is used for the nearby components which do reach higher temperatures. The heat distribution of these components is calculated and used to calculate the amount of heat radiating from these components.

4.3.2 Systematic bow error

The systematic bow error is a single calculation with the expected parameters. As the lens elements and the to be calculated errors are axisymmetric, it is possible to use an axisymmetric model. The geometry of the model can be seen in figure 28, the highlighted blue domain shows the beam area, which is exposed to heat radiation from the bottom. The two lens elements are parted by vacuum and supported on the right hand side (as the model is axisymmetric this is equal to a ring shaped support). The elements will be actively cooled to keep the temperature on the edges stable at 20°C. Both elements will be charged to the required potential and the steady state deflection is calculated.

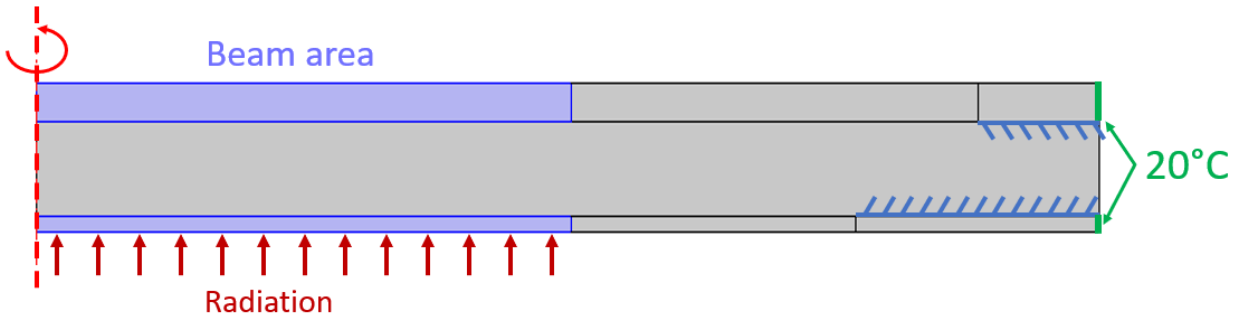

Figure 28: Geometry of the axisymmetric FEM model (not to scale)

The steady state deflection of the lens element with all boundary conditions is shown in figure 29a. Each line shows a different thickness of the lens element where the highest deflection (the blue line) is the thinnest element. The focus plane is only influenced by the deflection of the beam area, not the entire lens element. Therefore figure 29b shows the relevant beam area. Unfortunately the deflection of the thickest elements that fits inside the volume budget is too large to compensate by adjusting the geometry. Therefore the volume budget and the lens element thickness have been increased.

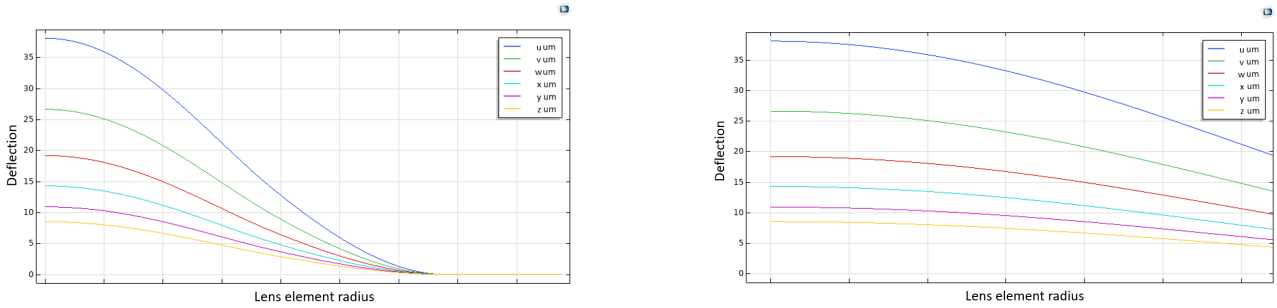

(a) Bottom lens element deflection

(b) Bottom lens element beam area deflection

Figure 29: Bottom lens deflection for multiple thicknesses (units removed for IP purposes)

4.3.3 Random bow error

The random bow errors are caused by the tolerances on the values of the systematic bow errors. To calculate the effect of these tolerances the caused bow error is calculated for each individual error source. The bow error for the top and bottom element can be re-calculated to a focal plane error using equation 1. This equation uses a subtraction of the top and bottom bow error to calculate the focal plane error. If the top and bottom error are independent they can theoretically be added by using the root mean square. However, in practice the root mean square addition is usually too optimistic, therefore the error will be calculated as half the RMS value and half the linear addition. Whether an error source is either dependent or independent will be explained below. By comparing the focal plane error of each individual error source the most critical tolerances can be identified.

Force

The elements bend due to electro-mechanical forces caused by a difference in potential between the two lens elements. The force caused by the potential difference is a distributed force which can be calculated using the electrostatic Maxwell stress tensor 5a. As the lens elements are a simple case with a constant electric field the equation can be simplified to 5b where σ is the distributed force in Pa, ε_0 the vacuum permittivity in Fm^{-1}, U the potential difference in V and t the distance between the elements in m.

$$\sigma = \varepsilon_0 E \otimes E - \frac{1}{2}\varepsilon_0 (E * E) * I \qquad (5a)$$

$$\sigma = \frac{\varepsilon_0 U^2}{2t^2} \qquad (5b)$$

The potential is controlled by electronics, they will charge the elements to a chosen potential with a certain tolerance that is specified by the manufacturer. The thickness is determined by the manufacturing tolerances of the spacer and the thickness of the bonding layer. The spacer is machined out of borosilicate glass, which requires grinding and polishing, both these techniques allow for very high tolerances. By mixing the adhesive with beads the layer thickness can be controlled very accurately, also minimizing the total thickness error. With data from the manufacturers and ASML experience an estimate is made for the tolerance on the total stack thickness.
Using the Comsol model the potential difference and spacer thickness are evaluated over the range of the expected tolerances. This results in a bow error for both the top and bottom element which are re-calculated in a focus plane error. This error source has an equal influence on both the top and bottom lens element, therefore the bottom and top element bow error are dependent.

Radius

The radius of the spacer determines the length of the suspension of the element (the r_0 in equation 2a). The error on this dimension is determined by the production tolerances of the spacer. As mentioned above the spacer will be machined out of borosilicate glass where the fine tolerances will be reached using grinding and polishing, which are very accurate production methods. Using the manufacturer data that was used for the spacer thickness the focal plane error caused by spacer radius error is calculated using the Comsol model. The spacer is a single part which supports both elements, therefore the bow error caused on both elements are dependent on each other.

Element thickness
The element thickness is determined by the tolerances of the wafer supplier. As explained in figure 23 there are 2 different values which influence the wafer thickness, total thickness and TTV. The thickness together with its tolerance indicate the maximum and minimum values of the wafer, the TTV indicates the thickness difference within one wafer.
Usually the tolerance on the total thickness will be significantly larger than the TTV tolerance (think in the order of 5 to 10), however it is possible to compensate for the total thickness. By depositing a layer of silicon or etching for short amounts of time single atom layers can be removed or deposited on the wafer. With this method it is possible to very accurately change the total thickness of the wafer, however as this process happens over the entire surface of the wafer at the same time TTV errors cannot be compensated. Therefore the focus of this error source will be on errors caused by the TTV.
The TTV has been covered in the non axisymmetric error section, however depending on the shape of the TTV the caused error can be axisymmetric. In figure 30 two thickness measurement of wafers are shown, in the left image the wafer has the shape of a valley, while on the right image it shows a more linear behaviour. The diameter of these wafers is significantly larger than the lens elements, therefore it is possible to select the best suited area on a wafer. Multiple elements will be created out of a wafer and the best of these elements will be selected. This will reduce the value of the TTV and also gives the option to select a TTV which result in a bow error instead of a non axisymmetric error.

Figure 30: Two 6" wafer thickness measurements from a wafer supplier (units are in μm)

While assuming that the TTV is perfectly axisymmetric, the thickness is varied in the Comsol model with a range that corresponds to the TTV tolerance provided by the manufacturer (the TTV tolerance is adjusted for the smaller diameter that is needed). This error will be independent for the bottom and top lens element, therefore in the calculation for the focal plane error they can be added with the combination of the root mean square and linear addition.

Hole size & taper
The holes in the beam area introduce a less rigid section to the lens elements. To reduce computation time this has been modelled by using an effective Youngs modulus. The holes will be created by a Bosch etch (see figure 31), by repeating a downwards biased etching step together with an unbiased passivation step a large etching depth can be reached. A general rule of thumb for the maximum etching depth of a Bosch etch is 10 times the feature size. When holes are created using etching instead of conventional methods like drilling or laser cutting, relatively little residual stress is created. This makes the element behaviour more predictable which is desirable.

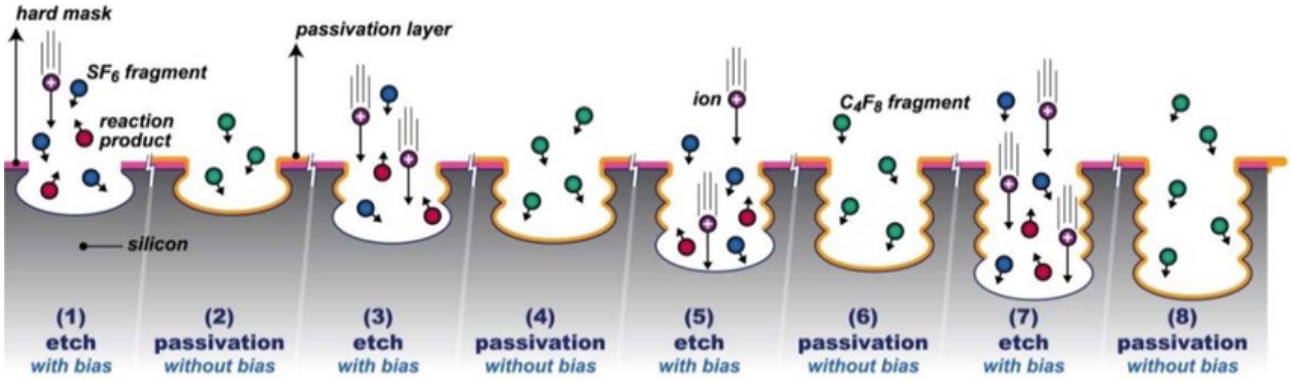

Figure 31: Steps in Bosch etching process [11]

There are two errors in the Bosch etching process which will have a large influence on the bow error, the hole size and taper. The top side hole size is determined by the lithography step, this is a very accurate process and thus results in a relatively small error. The depth of the hole is reached by etching multiple steps. A common occurrence during this process is hole taper. In the perfect case the walls of the hole will have a perfect 90 degree angle with the top surface, this value will however also be subject to a certain tolerance. Thus, there will be an error on the hole size due to lithography and an error on the taper due to the etching.
As the effective Youngs modulus model is 2 dimensional a true taper cannot be incorporated into the model, therefore a simplification is used. The decrease in stiffness due to the taper will approximately be the same as half the decrease in diameter (see figure 32). With this simplification the total diameter error can be calculated by adding the top diameter error with half the taper diameter error. Using the effective Youngs modulus model mentioned earlier in this chapter a maximum and minimum effective Youngs modulus is calculated, which in turn can be used to calculate the bow error. Both lens elements have a different thickness and will therefore be manufactured in separate batches, therefore this error is independent.

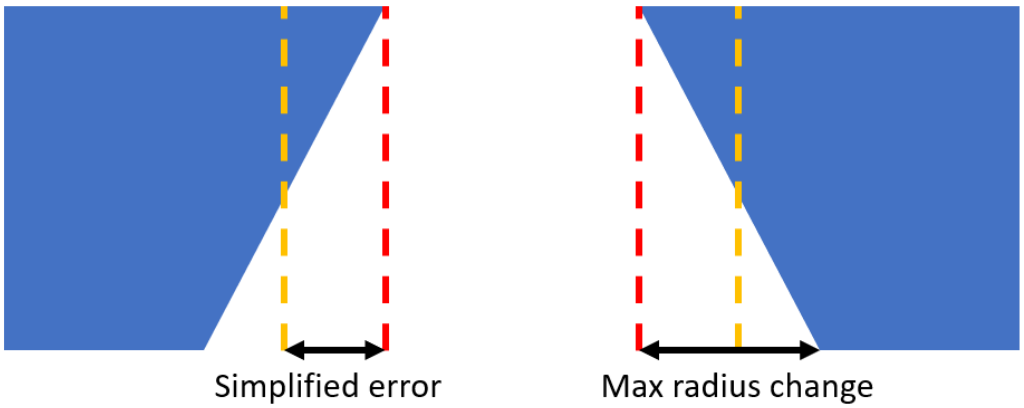

Figure 32: Taper error simplification to radius error (section view of a hole)

The calculated focal plane error due to hole size and taper was too large for the budget, however it can be slightly compensated. The largest contributor to this error is the taper, which is defined as a 90 degree angle with a tolerance. The stability of the error within this budget is however a lot better, meaning that if the manufacturer is allowed to choose the mean, the tolerance can be a lot better. Using experience from previous projects the calculation is repeated with the best values that have been reached.

Wafer bow
The lens element will be produced out of standard silicon wafers, in the data provided by the wafer manufacturer a lot of tolerances are mentioned, one of these tolerances is the wafer bow. This is a value which (for high quality wafers) is usually in the range of a few micrometer. Most wafers are however significantly larger than what is needed for the lens elements. Often the shape of this bow is (very close to) spherical, so using some trigonometry the wafer bow can be recalculated for a smaller size wafer. This value can directly be added to the bow error and is independent for both lens elements.

Thermal expansion
There are multiple active components inside the SEM which have heat as a byproduct, one of those components is located underneath the lens stack. In figure 28 the direction of the largest heat radiation source is shown. The radiation will cause the elements to heat up and expand, which in turn will change the focal plane. As long as the temperature remains stable the focal plane error will not change and will thus cause a systematic error (which will be taken into account for the systematic error budget). Therefore, this calculation will mostly focus on temperature stability instead of the actual temperature. The effects of the radiation are simulated by modelling the heat source and exposing the lens elements to the generated radiation. The wafer bow error caused by thermal expansion is dependent for both elements (same heat source for both elements), however, as the top element will barely increase in temperature the dependence does not matter.
The first calculations showed that the amount of heat generated in the source during SEM operation caused the component to become too hot. Therefore new power requirements were defined for the active components based on the cooling calculations made for this model, with these new requirements the amount of generated heat is reduced. The calculations yielded a requirement for the maximum temperature and temperature stability for the active components located underneath the lens element.

Element bonding
The elements will be connected to the spacer using an adhesive mixed with beads. The method of bonding will have a few effects which cause an error on the focal plane.
A suspected cause of focal plane error is pivoting around the inside bead, see figure 33. As the element bends inwards a moment is applied to the bonding, the bead wont allow the adhesive to be compressed, therefore the element will pivot around it and stretch the adhesive on the outside. This effect will increase the bow of the elements as the mounting would change from a clamped suspension to a lower stiffness hinged suspension.

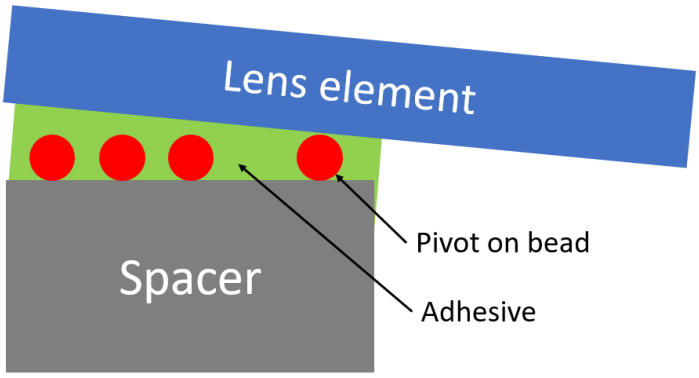

Figure 33: Lens element pivoting on the inside bead

To calculate the effect of the pivoting around a bead a model is constructed where the lens element is allowed to pivot around its inside edge. The stiffness of the support is adjusted to the Youngs modulus of the adhesive and the layer thickness is varied. In all cases of layer thickness the bow error caused by pivoting was small enough to be negligible.
The adhesive is also subject to the numerous effects described in chapter 3.1.2 (drift, shrink and hygroscopic swelling), the bow errors caused by these effects are however very difficult to calculate. In the next chapter an experiment will be described to test the effect of drift under shear load, unfortunately there is not enough time to test all the above described effects.

Overview
The quantitative error estimate shows which errors contribute the most to the total random bow error. In figure 34 the percentage of the budget that is required for each error is shown. As the different errors are independent on each other they can be calculated by adding half the linear and half the RMS value. The major contributors are the spacer thickness, element thickness and the hole size & taper. If the current numbers are added about 32% of the total budget is used, however, element bonding will most likely be the largest contributor of all and is still unknown.

Error source	% of budget (linear)	% of budget (RMS)
Potential stability	0.0	0.0
Spacer thickness	14.0	8.7
Spacer radius	0.5	0.0
Element thickness	10.0	4.4
Hole size & taper	14.5	9.3
Wafer bow	1.0	0.0
Thermal expansion	0.4	0.0
Element bonding	Unknown	Unknown
Total:	40.4+Unknown	22.5+Unknown
½ linear + ½ RMS	31.5 + Unknown	

Figure 34: Random bow error contributions

4.3.4 Non axisymmetric error

The non axisymmetric errors have the smallest budget as they cannot be compensated. The Comsol model used for the previous calculations is an axisymmetric model, therefore this model cannot be used to calculate these errors. A new model 3D model is constructed with the same basic geometry as before (this model is essentially the same, but does allow non axisymmetric features at the cost of computation speed). This model is used to calculate the following errors:

Non axisymmetric thickness
As explained in the random bow error estimation the TTV is the change of thickness in a single lens element. Preferably the TTV will have an axisymmetric shape, which will cause a bow error instead of a non axisymmetric error. As this will not always be the case the effect of a non axisymmetric TTV is calculated.
The shape of the TTV will always be smooth (as the wafer is carefully polished). On top of that the worst TTV distributions will not pass the selection (as explained with the random bow error, the best elements will be selected). Therefore, from the most likely TTV distributions a linearly increasing thickness (see figure 35) is the worst case for causing a non axisymmetric error.

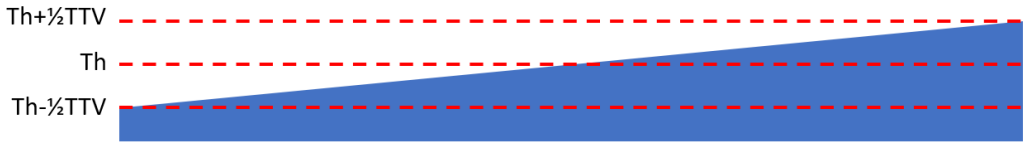

Figure 35: Linearly increasing TTV

To properly show the non axisymmetric effect the curves are imported into Matlab and the pure bow (no error) is subtracted from the different TTV errors. This yields the pure non axisymmetric error, which can be seen in figure 36a. As explained in chapter 4.1 vertical and tilt errors can be compensated by adjusting the wafer, therefore it is possible to adjust this graph in height and angle. An optimization algorithm is programmed in Matlab to find the optimal values for the vertical and tilt compensation, one such line can be seen in figure 36b. The result of all the compensated errors can be seen in figure 36c, this compensation decreased the error by roughly 40%.

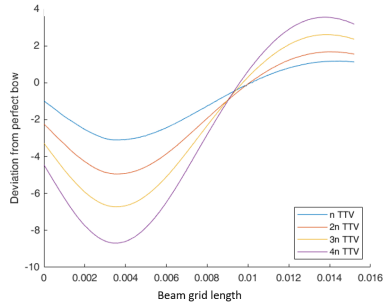

(a) Non axisymmetric error caused by TTV

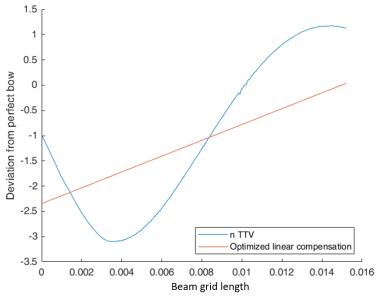

(b) Optimized linear equation to compensate TTV error

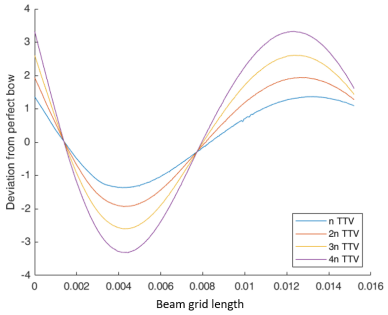

(c) Compensated TTV errors

Figure 36: Linear compensation process for TTV errors (units removed for IP purposes)

Beam area misalignment

The beam area misalignment has already been lightly covered in chapter 3.1.2. The hole grid in the beam area introduces a less rigid spot in the lens element, when this spot moves around the curve of the element changes. The amount that the spot moves around is defined by the XYRz alignment tolerance.
The error is calculated using the same process as before, first the bow curve is calculated in Comsol, then the deviation from the perfect bow and an optimal linear compensation is calculated using Matlab. The process can be seen in figure 37, especially after compensation the numerical noise becomes rather present. This can be explained by the size of the error, the TTV error from figure 36 are an order of magnitude larger, therefore the noise is a lot less visible in this plot. After compensation the non axisymmetric error due to beam area misalignment is reduced by about 80%.

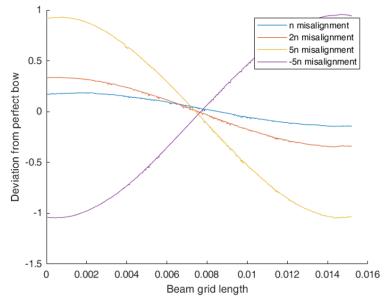

(a) Non axisymmetric error caused by beam area misalignment

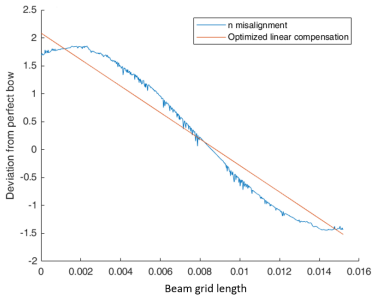

(b) Optimized linear equation to compensate beam area misalignment

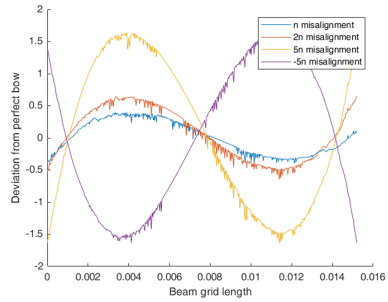

(c) Compensated beam area misalignment errors

Figure 37: Linear compensation process for beam area misalignment (units removed for IP purposes)

Non axisymmetric hole size

In the previous chapter the effect of the change in hole size and taper is covered, it is explained that the change in taper can be translated to a change in diameter, allowing both errors to be covered by one variable. Using the effective Youngs modulus model the size of the holes is recalculated to an effective Youngs modulus, which can be implemented in the model.

The holes in the wafer are created simultaneously, therefore the variation of hole sizes and taper within a single wafer will be significantly smaller than the total tolerance on these parameters. However, some variation will still be present within the wafer which can cause a non axisymmetric error.

The largest non-bow error is created when the most extreme hole sizes are on opposite edges of the grid. The holes are created in a single process, therefore the difference between adjacent holes will be minimal. Therefore the largest non-bow error will be caused with a linearly increasing or decreasing hole size. This will cause a changing effective Youngs modulus along the beam grid, which will result in a non axisymmetric error.

Comsol assigns the Youngs modulus to a material, which in turn is assigned to a domain, therefore it is very difficult to implement a gradient Youngs modulus. This problem is circumvented by cutting the beam area in 7 separate areas, each with an assigned material and thus Youngs modulus (see figure 38). This model allows the Youngs modulus to be changed throughout the grid simulating a changing hole size and taper.

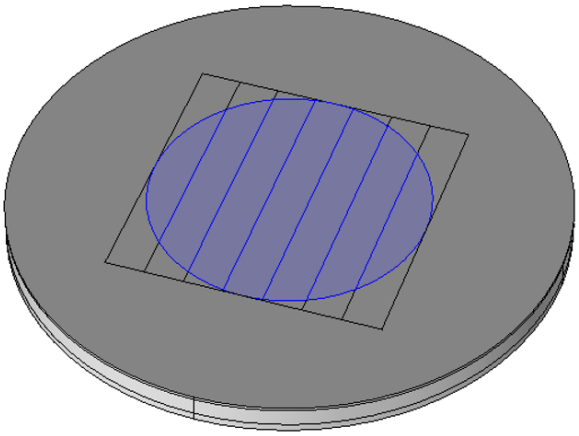

Figure 38: Material/Youngs modulus assignment

Again the deviation from a perfect bow is calculated and linearly compensated, this can be seen in figure 39. The linear compensation decreased the error by roughly 25%.

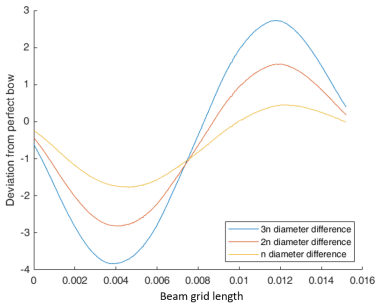

(a) Non axisymmetric error caused by hole size difference

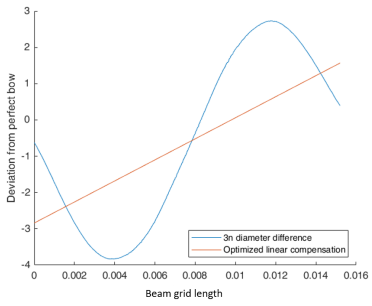

(b) Optimized linear equation to compensate hole size difference

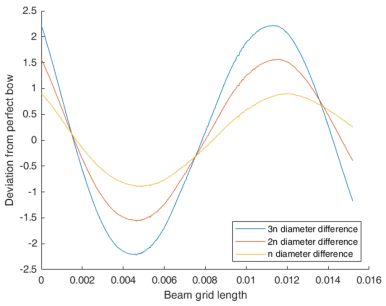

(c) Compensated hole size difference errors

Figure 39: Linear compensation process for hole size difference (units removed for IP purposes)

Spacer flatness

The force due to the potential difference is quadratically dependent on the distance between the elements. Therefore, a changing spacer thickness will result in a non linear change in force, which causes a non axisymmetric error in the bow of the elements and thus the focal plane. The deviation caused by this error, the compensation and the compensated result can be seen in figure 40. After compensation the error due to spacer flatness is reduced by about 70%.

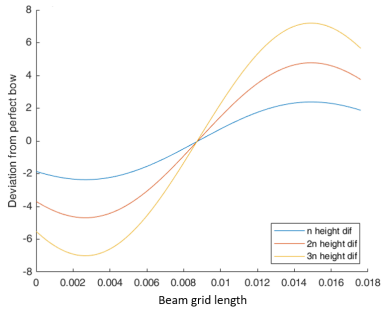

(a) Non axisymmetric error caused by hole size difference

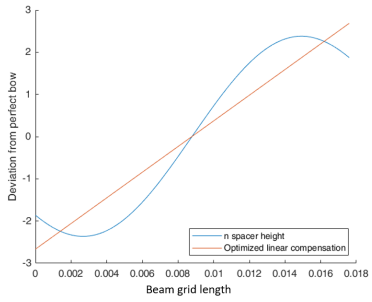

(b) Optimized linear equation to compensate hole size difference

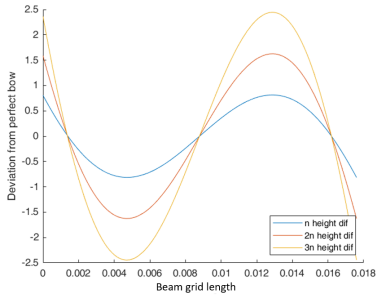

(c) Compensated hole size difference errors

Figure 40: Linear compensation process for spacer flatness (units removed for IP purposes)

Element bonding

Unfortunately the same problems are encountered as for the random bow errors. Due to the difficulty of predicting polymers a proper quantitative estimate can not be made. This will require further testing and will be covered in the next chapter.

Overview

To put the sizes of the errors in perspective an overview is made in which the percentage of the budget that is required for each error source is shown (see figure 41). As the error sources are not dependant on each other the average of the linear and RMS error can be taken. It can be seen that the error due to beam area misalignment is negligible and that the major contributors are the thickness, hole size and spacer flatness. Before the linear compensation the full budget was not enough, after compensation of the errors the total error is about 58% of the budget. The size of the element bonding error is however still unknown.

Error source	% of budget (linear)	% of budget (RMS)
Thickness	33.2	25.6
Beam area misalignment	0.4	0.0
Hole size	22.2	11.4
Spacer flatness	16.3	6.1
Element bonding	Unknown	Unknown
Total:	72.1+Unknown	43.1+Unknown
½ linear + ½ RMS	57.6+Unknown	

Figure 41: Non axisymmetric error budget

5 Experimental

The effects of the tolerances on the lens elements are relatively easy to predict with FEM software, this is however not the case for the effects in polymers like adhesives. In chapter 3 the Tg of adhesives was unclear and numerous effects like drift, shrink and hygroscopic swelling were described. In this chapter it will be explained how the Tg and drift of the selected adhesives are tested. First it is explained why the Tg and drift are tested, next how they will be tested and finally how the data will be processed.

5.1 Experiment objective

Table 1 in chapter 3.1 shows how well different bonding methods score for the requirements. Adhesives scored high, except for 2 categories, the thermal conditions and the unpredictable effects mentioned in the remarks. How these effects influence the error budgets and requirements for the lens stack is difficult to calculate. Therefore, the clear up some of these uncertainties the glass transition temperature and drift will be tested.

5.1.1 Glass transition temperature

Many ASML machines are located in Asia. Therefore, it is not unrealistic that the lenses might pass through an airport located in the desert or other very hot locations. Standard shipping guarantees that the temperature of the transport does not exceed -20 to 60°C. However, if needed, special requests can be made for better temperature regulation of the package. When a sample heats up the larger thermal expansion of the borosillicate spacer will apply shear stress on the adhesive. On top of that the adhesive will lose strength as it heats up. If the increased load becomes larger than the decreased adhesive strength the lens will lose its alignment and curvature. On top of that the lower Youngs modulus due to the increase in temperature can significantly speed up the viscoelastic creep, causing drift and resulting in the lens losing its focus.
An adhesive manufacturer will often provide a Tg for the adhesive. However, the term glass transition temperature is not well defined as it is a range of temperatures. On top of that the recommended curing process might not be ideal for this implementation, changing the curing process to a better suited one might change the Tg too. Therefore, a test should be designed which allows the Tg of different adhesives and curing processes to be compared.

5.1.2 Drift

As mentioned before polymers are subject to a lot of different unpredictable effects like drift, shrink and hygroscopic swelling. These effects cause displacements in the order of nanometers, however depending on the direction the effect on the lens bow can be greatly magnified. Shrink and hygroscopic swelling cause the element to move up or down (although downwards movement will be limited by the beads) while drift causes the element to move inwards (see figure 42). When the entire element is moved up or down a random bow error is caused due to the changes in the electric field strength. However, as these movements are relatively small the error is expected to be minimal. When the elements drift inwards the bow can increase significantly due to the small deflection compared to suspension length (about 1:15.000 ratio of bow:suspension length). The ratio between lateral movement and increase in bow has been calculated in Comsol and resulted in a ratio in the thousands, where the ratio is heavily increasing when the element becomes more flat. Due to this ratio the effects that cause lateral movement will result in the largest errors. Therefore the focus of this experiment will be errors caused by drift.

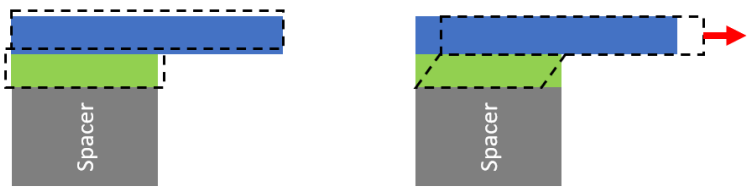

Figure 42: (left) swelling or shrink causes the element to move up or down, (right) drift or viscoelastic creep cause the element to move inwards

5.2 Glass transition temperature test

The goal of the test is to see which of the selected adhesives and curing processes result in the best Tg. In the industry thermal conditioned tensile testing machines are used (see figure 43). The machines can plot the stress strain curves for samples while in a temperature controlled environment. These machines deliver an absolute result for the strength of the adhesives at different temperatures. Unfortunately these machines are not present among the available measuring setups. Therefore, another setup is designed with the available equipment.

5.2.1 Design of experiment

The proposed test uses a bimetallic actuator and evaluates whether the ideal curve of the actuator is followed. When the bi-metal is heated the aluminium on the bottom will expand more than the silicon on the top, causing the element to curve upwards and apply a shear force on the adhesive holding the elements together (see figure 44).

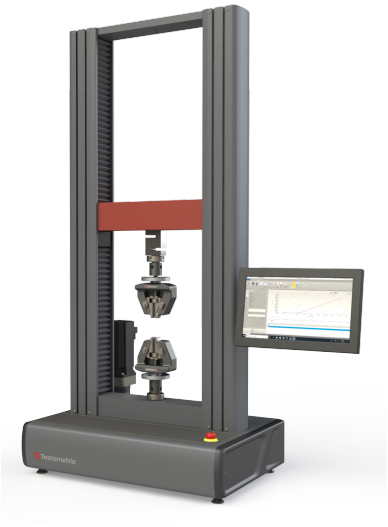

Figure 43: Tensile testing machine (not environmentally controlled) [13]

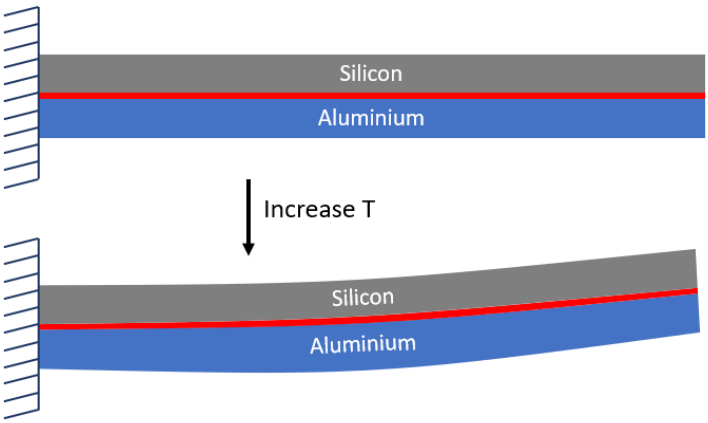

Figure 44: Bimetallic actuator

The shape of a simplified bimetallic actuator can be calculated using equation 6 [2]. This simplification assumes no elasticity in the bonding and does not account for stiffness in the metal elements. Therefore, the equation only holds for thin actuators, as the stiffness in thin elements will have a relatively small effect. The equation calculates the radius R of the bend bimetallic actuator with the thickness t and the difference in CTE between α_1 and α_2 (23.4e-6 and 2.6e-6 K^{-1} have been used for aluminium and silicon respectively). Using some trigonometry and the length of the actuator the travel distance of the tip of the actuator can be calculated using the radius R.

$$R = \frac{t}{\Delta T * (\alpha_2 - \alpha_1)} \tag{6}$$

This equation does not take into account the stiffness of the element, therefore, to validate the equation, the deflection has been recalculated in Comsol. It is also suspected that the low modulus of elasticity of the adhesive and the increased spacing of the elements due to the adhesive layer might influence the deflection. Therefore, to ensure a consistent layer thickness the adhesive is mixed with 50 micrometer beads, ensuring that the adhesive layer will be a constant thickness. The same Comsol calculation has been repeated with an adhesive layer between the elements, see figure 45. For a length of 50mm, a thickness of 1mm and a temperature difference of 40°C equation 6 yields a deflection of 1.04mm, Comsol yields 1.00mm and Comsol with an adhesive layer 0.949mm. The results were close enough that the equation is assumed to be roughly valid.

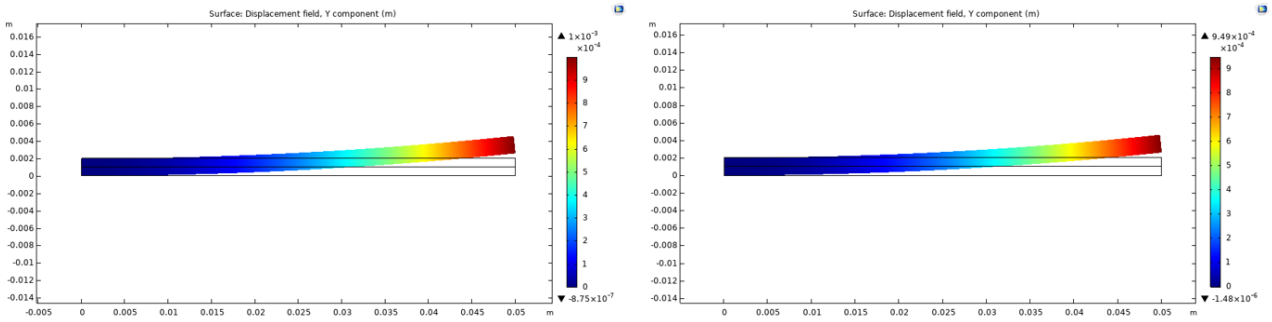

Figure 45: (left) vertical deflection of a bimetallic actuator, (right) vertical deflection of a bimetallic actuator with an adhesive layer

From the equation and trigonometry it can be concluded that the deflection is quadratically proportional to the length of the actuator and inversely proportional to the thickness (assuming small angles). Therefore, to get the maximum deflection the length should be maximized and the thickness should be minimized (within reasonable bounds).
The final actuator dimensions are a length of 100mm and a thickness of 0.5mm, this result in a deflection of about 4mm at 60°C (or a change of 40°C).

The final test setup can be seen in figure 46. The sample will be suspended above the heatplate (to approach homogeneous heating) while its temperature will be measured with a thermocouple. The sample will be video recorded while it increases in temperature. The deflection can be measured on the recording with the help of the reference scale located behind the sample.

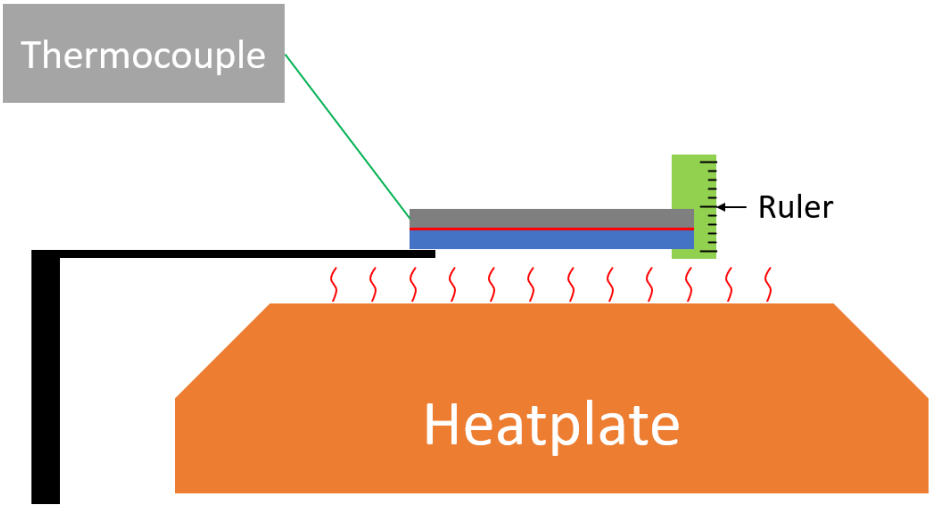

Figure 46: Tg test setup from the camera point of view

One of the goals of this test is to evaluate the effect of different curing processes on the Tg. A higher curing temperature will most likely increase the Tg, but this will usually come at the cost of alignment precision. To counteract the loss of alignment the curing processes shown in figure 47 are proposed. The first process is a simple room temperature cure. This will most likely result a worse Tg, but will have better alignment. The second process first 'tags' the elements with a room temperature cure, and is post-cured at a higher temperature. First the adhesive is partially cured at room temperature, next, the adhesive is cured at a temperature slightly lower than the Tg. During the curing the room temperature cured adhesive should be able to hold the element in place and ensure the alignment is preserved. Each of the 3 adhesives selected in chapter 3 will be tested with both curing processes.

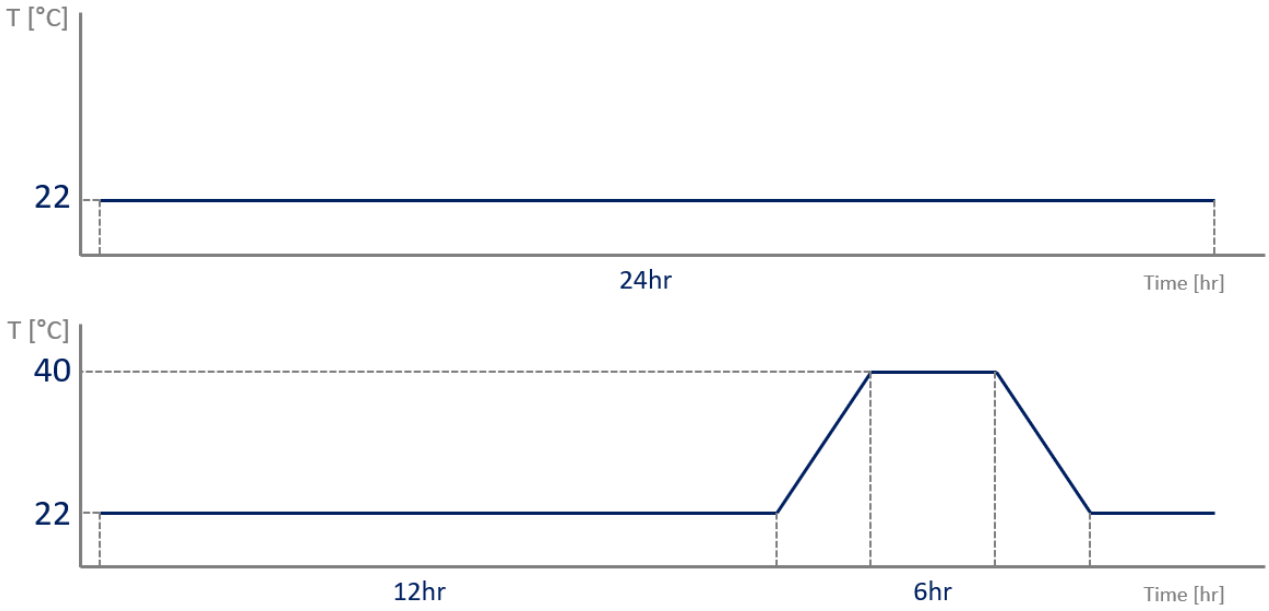

Figure 47: Curing processes for the adhesives

5.2.2 Data analysis

The Tg test will result in a video paired with a temperature measurement. The video can be used to read out the displacement of the tip of the bimetallic actuator (see figure 48). Together with the temperature measurement the video can be used to evaluate the performance of the adhesives.
The temperature measurements is coupled with the displacement and imported into Matlab. The data consists of a timestamp, a temperature and a displacement. by interpolating the data over a selected range of temperatures the measurements can be normalised resulting in a displacement for a range of temperatures. This allows the measurements to be averaged for each adhesive (there are multiple samples for each combination of adhesive, curing and layer thickness).

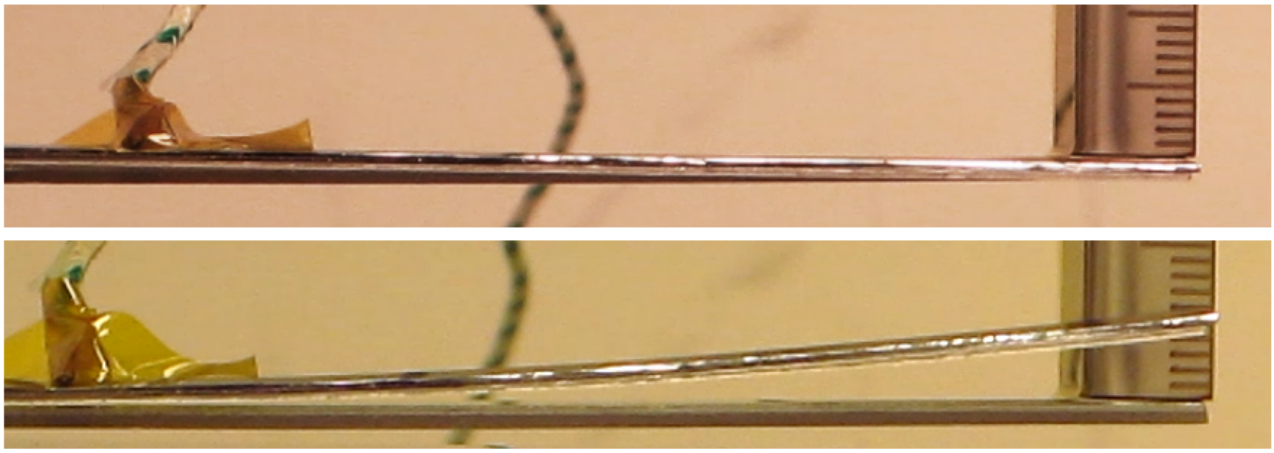

Figure 48: Actuator displacement at room temperature (top) and 70°C (bottom)

The tip of the actuator will exhibit a certain amount of displacement based on the temperature of the actuator. This will result in a curve which, if no failure occurs, should be straight (displacement and temperature are linearly dependant on each other). If the adhesive fails or loses strength the displacement will not linearly increase with the temperature, which will show as a flattening of the curve. Therefore the first derivative of the curve will give a good indication of the moment when the adhesives fails or loses strength.

5.3 Drift test

The goal of the drift test is to evaluate what magnitude of flatness error can be expected due to drift in the lens stack. The maximum acceptable error has been calculated in the random bow error estimate and resulted in a budget of a few micrometer. Using the ratio between lateral drift en resulting bow error the allowable drift is several nanometers. As drift is an effect that occurs over a long period of time, the setup has to be able to accurately measure over this time period.

5.3.1 Design of experiment

It is not realistic to measure a displacement of several nanometers over a long period of time because the measurement noise will likely be larger than the measured effects. However, the effect of drift on the lens elements is in the order of micrometers. Therefore, instead of measuring the drift the caused bow error is directly measured. Essentially a single simplified lens element and load are recreated and the bow error over a period of about 2 months is measured.

Three adhesives have been selected in chapter 3.1, each of these adhesives will be tested with a room temperature cure and a higher temperature cure. On top of that each option needs at least 3 samples to eliminate anomalies and show reproducibility. Due to the high number of samples needed it is not possible to mount a sensor above each sample. Therefore, a setup is constructed which allows samples to be placed inside a measuring setup. The used setup is a high accuracy XY stage with an optical height sensor (the measuring pattern is shown in the data analysis). The combined height error of the stage and measuring error of the optical sensor is about 5% of the maximum acceptable bow error.

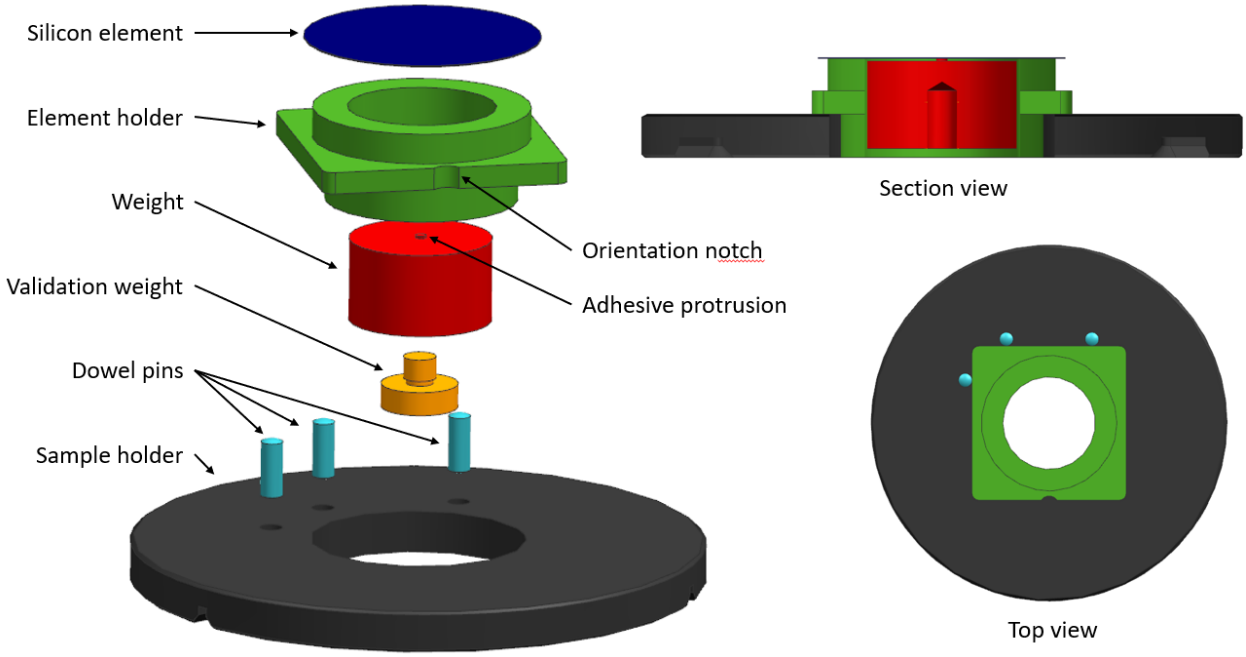

Figure 49: Setup of the drift test

The sample holder is placed on the XY stage and has three dowel pins on which a sample can be docked. A sample consists of a silicon element glued to an element holder, with a weight pulling the centre of the silicon element down. While the sample holder remains in the measuring setup the samples can be exchanged and measured one by one.

The weights will be lathed out of stainless steel, the sample and element holders will be machined out of aluminium. Stainless steel is chosen due to its high density and cleanroom compatibility, aluminium for its ease of machining and availability. Unfortunately the aluminium sample holders introduce an issue: aluminium has a CTE that is significantly higher than silicon. The actual spacers will be constructed out of borosilicate glass, machining this material requires grinding which is expensive and has very long lead times. To stay within the available time for this research the parts are milled. Unfortunately there were no metals available with a comparable CTE to silicon. The effect of the CTE difference is expected to be minimal for the room temperature cured samples, however this is not the case for the 40°C curing. If the samples are rigidly connected to the aluminium spacer they will break at a temperature of about 45°C. Therefore the curing scheduled introduced for the Tg test will be slightly adjusted to 30°C for the drift test samples.

Simplifications

There are a few necessary simplifications in the setup compared to the actual elements. The actual elements will have a beam area filled with a grid of holes. It is not realistic to create a batch of these elements with a hole grid within the available time and budget. The lack of hole grid will cause a change in rigidity and shear load on the bonding, this will have to be compensated for.
Another simplification is the load. The actual load is caused by a difference in potential. With the time available it is not possible to build a safe setup where a potential difference of tens of kV's can be supported. Therefore, the load has to be applied with a different method.

Common ways of applying distributed loads use either liquids or gas. When a liquid is deposited on top of the element a distributed load will press it down, when a higher pressure is applied above the element or a lower pressure underneath the element a similar force can be recreated. Unfortunately both methods have a few problems. the available measuring setup requires the samples to be measured from the top, therefore if either a liquid or a pressure chamber is located on top of the element a different measuring setup is needed. A lower pressure under the element is still a good option. However, this will require an air tight pressure chamber which are prone to leak, potentially causing an unstable load on the element. Distributed loads seem unfeasible, therefore point loads are considered. By gluing a weight underneath the lens elements a constant downwards point force can be applied to the element. A drawback of this method is sensitivity to G-forces, any rough handling can greatly change the load on the element, but with careful handling the G-forces should be minimal.

Optimization

There are two variables which should be recreated as close as possible to the actual case, the shear load and the curvature. The amount of drift depends on the distributed load that is applied. Therefore, to mimic the real stack the load should be comparable. The curvature determines the ratio between lateral movement and change in bow. If the element is very flat, small amounts of lateral movement result in large changes in bow (see figure 50). Therefore a smaller bow results in a larger amplification factor between lateral movement and change in bow.

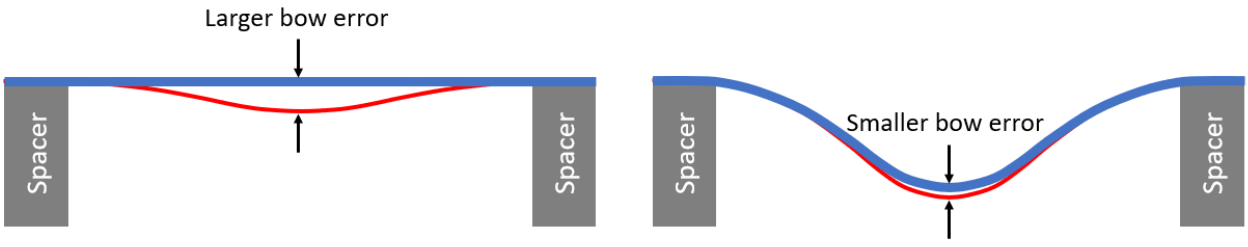

Figure 50: The same amount of lateral movement can result in different bow errors depending on the curvature of the element

The benefit of mimicking the actual lens element is that it prevents the need to recalculate measurements to bow errors. This is however only the case when the curvatures of the elements are roughly the same. Therefore the test setup should be designed to have a similar curvature as the actual elements.
The lack of a hole grid introduces a problem, the less rigid beam area changes the curvature of the element in a way that cannot be reached with solid elements (see figure 51a). The deviation of the curves compared to the original element with hole grid are calculated by subtracting the original curve from the calculated curves and can be seen in figure 51b. Either the element is stiff enough on the sides and too weak in the centre or vice versa.

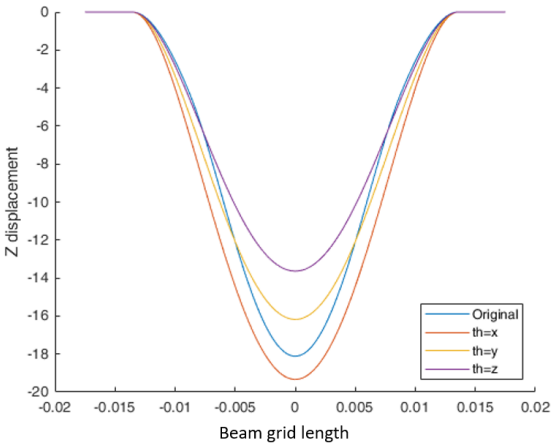

(a) Curves of solid elements with different thicknesses compared to the element with beam grid

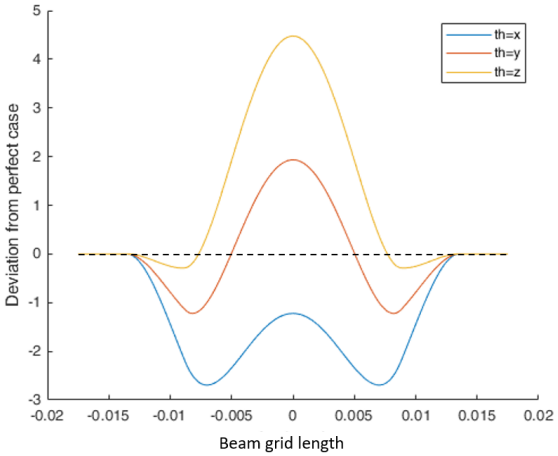

(b) Errors of solid elements with different thicknesses compared to the element with beam grid

Figure 51: Effect of the hole grid on the curvature of the element compared to solid elements

The load that is applied can be varied to compensate the deviation caused by the lack of hole grid, changing this force allows the curve to be adjusted at the cost of changing the shear load on the bonding. By changing the element thickness and the applied load the test setup can be adjusted to fit the actual case as good as possible. The choice in element thickness is limited to the stock of the wafer manufacturers, two possible thicknesses are available that have a comparable curvature to the original element. For both thicknesses the force is varied and the error of the curvatures is plotted. The best combinations of available thickness and force can be seen in figure 52, the largest error of the curves is about 5% of the total bow.

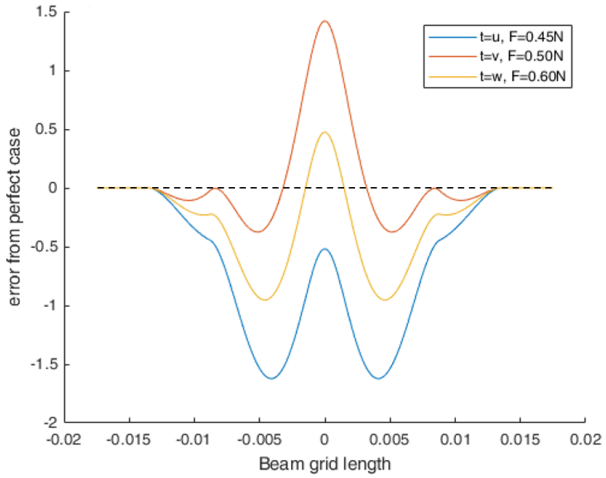

Figure 52: Error of best thickness and force combinations

For the best fit with the available wafer thicknesses more force has to be applied than the original distributed force, which will likely result in a higher shear stress for the bonding. To compensate this the bonding area is increased (more bonding area equals a lower average shear stress), this is however not a one on one relation. Although the extra bonding area does decrease the average shear stress it does not necessarily decrease the maximum stress (which is dominant in the caused drift), see figure 53. The average shear stress (black dotted line) decreases with the larger bonding area, while the maximum shear stress did not (this is however an extreme case). An increase in surface area will usually decrease the maximum shear stress, but it is usually not proportional to the increase in surface area.

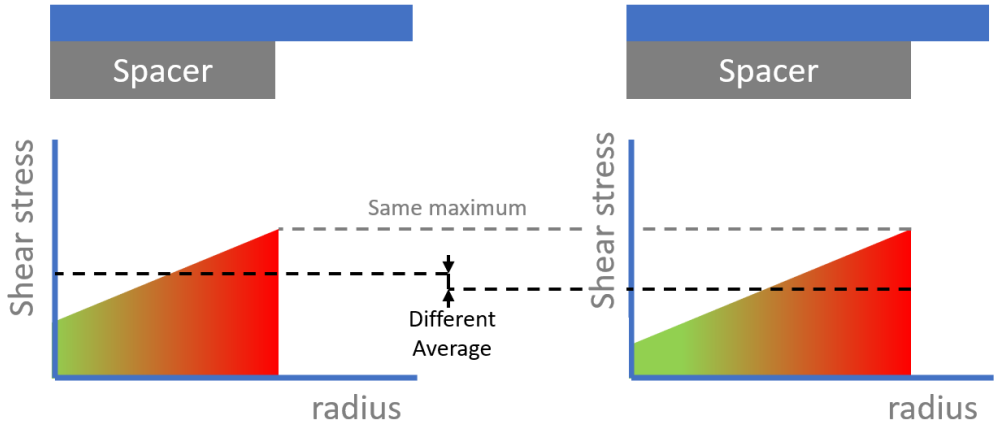

Figure 53: A decrease in average shear stress does not necessarily mean a decrease in max shear stress

The bonding surface area is increased, reducing the average shear load until it is twice the original shear load (resulting in a safety factor of 2). Therefore, if an acceptable amount of drift is measured in the test setup, the actual lens element will most likely also have an acceptable amount of drift.

5.3.2 Data analysis

The data for the drift test will be acquired using an XY stage and optical sensor, which will yield XY coordinates with the corresponding height measurement. For the measurement a pattern of points is selected which will be measured by the setup (see figure 54).

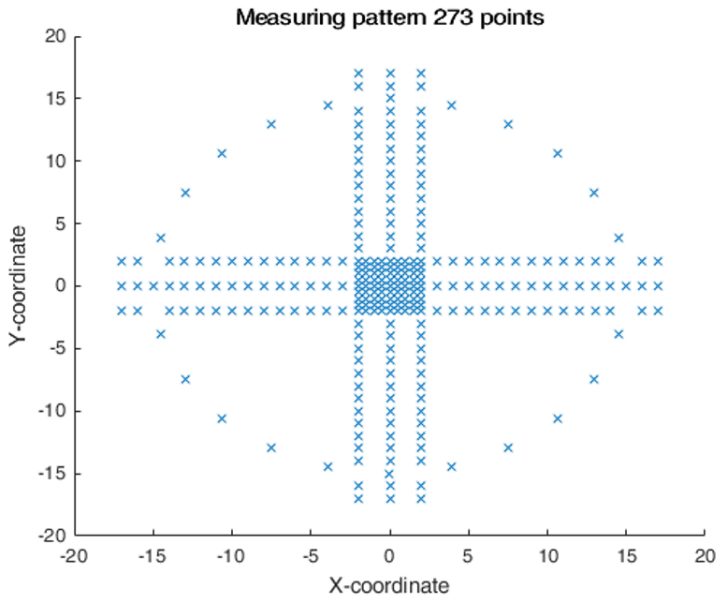

Figure 54: Measurement pattern drift test

As multiple samples are measured the samples will be exchanged on the sample holder. If during the displacement a particle gets caught between the samples and the sample holder the measurement points will be skewed, on top of that the stage will also not be perfectly flat. To compensate these errors a circle of points is measured on the element support. These points form a plane that can be subtracted from the measurement, ensuring a bow measurement relative to the element edges and compensation for errors caused in the stage and by sample replacement.
The dense square in the centre ensures that the deepest point is accurately measured. The bow of the wafer will have its deepest point located inside this grid. If the deepest point is located between multiple measured points an error is caused (the actual lowest point will be lower than the measured lowest point). The density of the grid is determined by this error, with this density the maximum potentially caused error when the lowest point is between two measurement points is at an acceptable level. Therefore, the accuracy of the sample placement and the stage (the total XY error) can only create a minimal measurement error as long as the deepest point is located within the fine grid.
The straight lines of points will show the curvature of the element. This can be used to find the source of measurement errors by showing the actual shape of the element instead of just values.

A Matlab script is written which reads out the data and analyses it. First a plane is fitted to the ring of data points (see figure 55), this will compensate any plane errors. After the plane is subtracted from the data points the lowest point and its position are calculated.

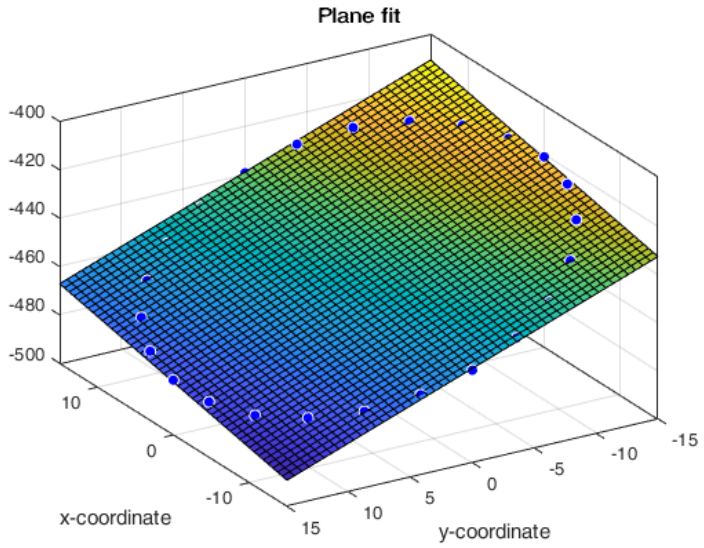

Figure 55: Plane compensation

Drift is an effect that occurs over a long time span. With the available time in mind a measurement time of about 2 months is chosen. During these 2 months a height map will be made of the samples every week. The results will be processed in Matlab where the lowest point will be calculated.

6 Results & Discussion

In the following chapter the results from the previously described tests are shown. For each test the results, issues, fixes and how to continue further testing are discussed. First the glass transition temperature test is covered, followed by the drift test.

6.1 Glass transition temperature test

There are 8 combinations of adhesives, curing and layer thickness that will be tested. Each of the three selected adhesives will be tested with both curing processes, on top of that glue 1 will also be tested without beads.

6.1.1 Results

For each category at least 3 samples were tested. The results were normalised in Matlab and then averaged for each category. The averaged measured displacement of the actuator tips and its derivative are plotted for all adhesives as a function of the temperature in figure 56. The tip displacement is linearly dependant on the temperature of the actuator. Therefore, as long as the adhesive holds, the graph should be a straight line. When the adhesive fails it is unable to keep the elements connected, allowing them to shift relative to each other and resulting in a decrease in tip displacement. Therefore, adhesive failure will be indicated by a sudden decrease in tip displacement and a sharp decrease in slope. The ideal case displays the calculated tip displacement using equation 6. This line would result from an ideal bimetal actuator without any stiffness in the elements and an infinitely stiff bonding (in shear direction). Because the actual actuators have stiffness and a relatively soft bonding the slope of the actuators is less steep than the ideal case. It is theorized that this effect is the cause for the early failure of the samples without beads.

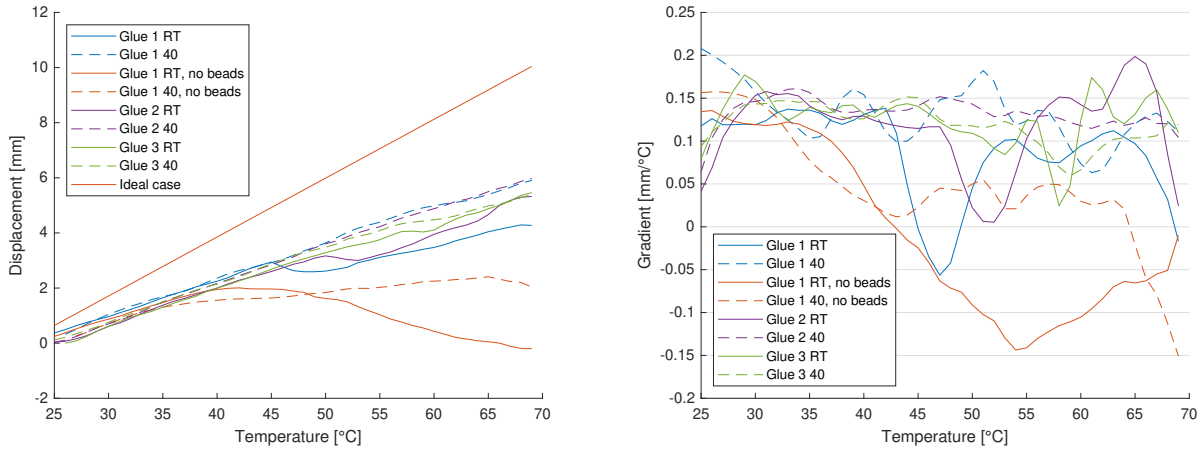

(a) Actuator tip displacements

(b) Actuator tip displacement derivatives

Figure 56: Actuator tip displacements and derivatives as a function of temperature

Due to number of different combinations that have been tested the figure is difficult to read. Therefore, each adhesive will be plotted individually. Glue 1, glue 1 without beads, glue 2 and glue 3 can be seen with their standard deviations in figure 57, 58, 60 and 61 respectively.

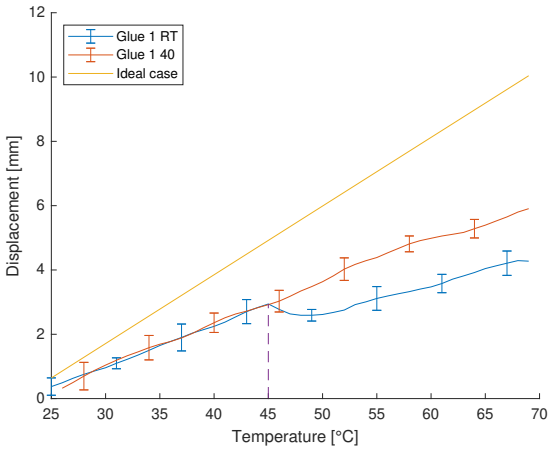

(a) Actuator tip displacements of glue 1

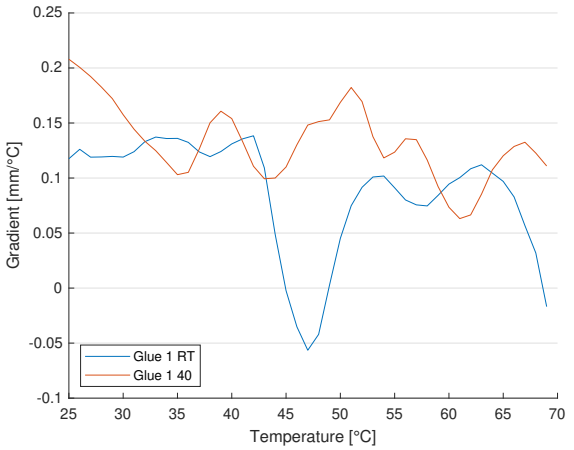

(b) Actuator tip displacement derivatives of glue 1

Figure 57: Actuator tip displacements and derivatives as a function of temperature for glue 1

The actuator tip displacements and the derivatives of glue 1 are plotted in figure 57. Glue 1 shows a clear difference between the room temperature cured samples and the samples with a 40°C post cure. Where the room temperature cured samples display an actual decrease in tip displacement around 45°C the post cured samples remain a roughly straight line. The datasheet provided a Tg of 50°C for glue 1 with a room temperature cure.

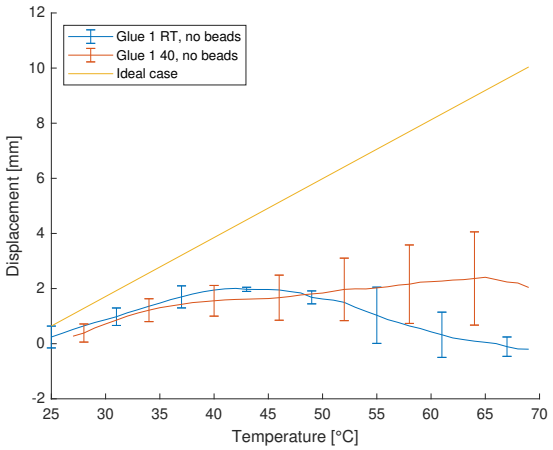

(a) Actuator tip displacements of glue 1 without beads

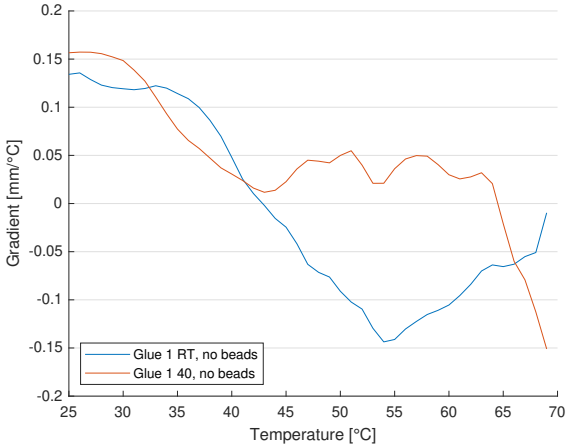

(b) Actuator tip displacement derivatives of glue 1 without beads

Figure 58: Actuator tip displacements and derivatives as a function of temperature for glue 1 without beads

Figure 58 shows the actuator tip displacements and derivatives of glue 1 without beads. The samples without beads show an early failure at a temperature of about 35°C with a very poor reproducibility (the error bars are relatively large). The beads inside an adhesive define the layer thickness of the bonding. Without beads this layer is theoretically zero while the adhesive fills up any cracks and crevices between the two elements. It was theorized that due to adhesive shrink the elements would be strongly pulled together, creating a friction force between the elements. However, this test showed that the this theory does not hold, at least not for displacements of this magnitude.

Because no element is perfectly flat the thickness of the adhesive layer will vary along the surface of the bonding. This variation is relatively small when the adhesive layer is 50 micrometer thick, however, for a layer without beads the variation will be significant (see figure 59). When a shear force is applied on the thicker adhesive layer the load will be evenly spread among the bonded surface. When a shear force is applied to the thin adhesive layer the load will first be concentrated at the thinnest part of the bonding (as it can elastically deform the least). The load concentration will tear the adhesive layer at that point, and move the load concentration further along the bonding. This will continue until the complete bonding fails.

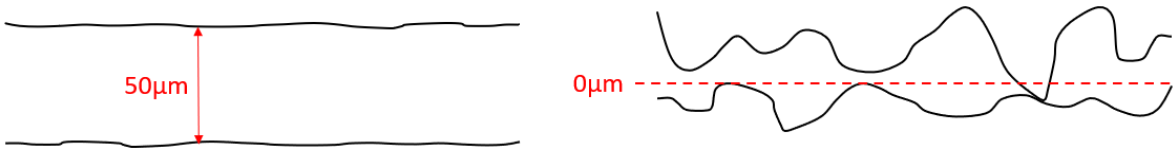

Figure 59: Adhesive layer thickness with and without beads

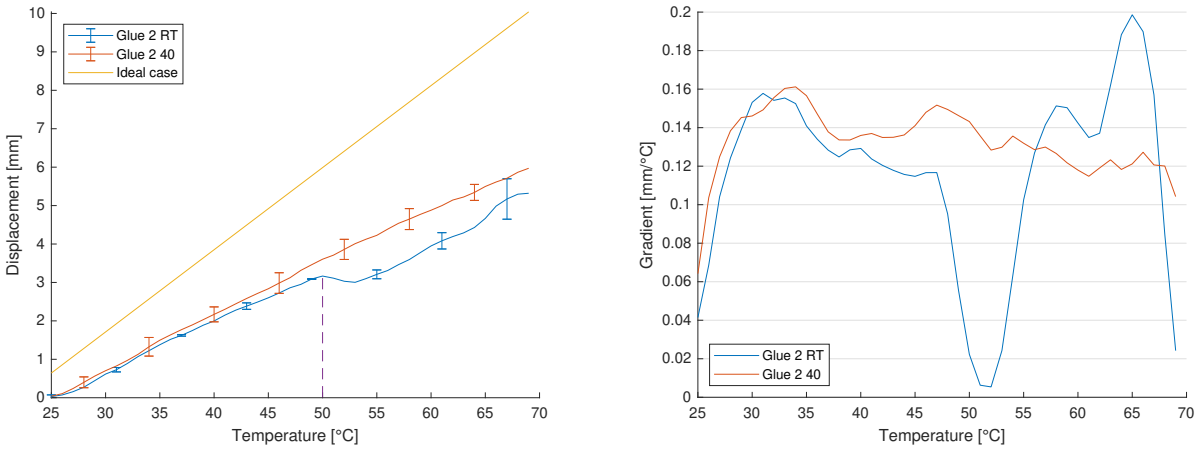

(a) Actuator tip displacements of glue 2

(b) Actuator tip displacement derivatives of glue 2

Figure 60: Actuator tip displacements and derivatives as a function of temperature for glue 2

The actuator tip displacements and the derivatives of glue 2 are plotted in figure 60. Just like glue 1 the room temperature cure shows a clear failure point while the post cured samples follow a relatively straight line. The slope of the room temperature cure of glue 2 decreases around 50°C, this corresponds with the 49°C Tg provided by the datasheet.

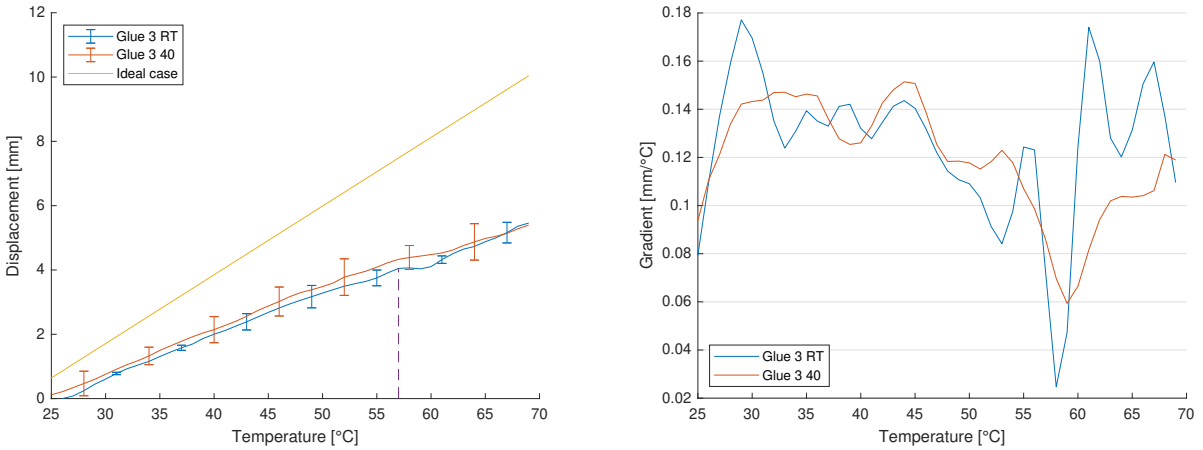

(a) Actuator tip displacements of glue 3

(b) Actuator tip displacement derivatives of glue 3

Figure 61: Actuator tip displacements and derivatives as a function of temperature for glue 3

The actuator tip displacements and the derivatives of glue 3 are plotted in figure 61. This adhesive shows very little difference between a pure room temperature cure and a 40°C post-cure. The first large decrease in slope is measured around 57°C for both curing processes. Although the size of the decreased tip displacement due to the failure is smaller than in the other adhesive failures.

As manufacturers use different definitions for the Tg it is difficult to compare those values. This test does not yield an absolute Tg as the amount of shear force is not properly controlled. However, it does allow the performance of the adhesives to be compared. The performance for each combination of adhesive, curing and layer thickness can be seen in table 3 as an effective Tg (a true Tg is only dependent on the adhesive and curing, not the presence of beads).

Combination	Effective Tg* [°C]
Glue 1, RT curing	~45
Glue 1, 40°C curing	70+
Glue 1, RT curing, no beads	~40
Glue 1, 40°C curing, no beads	~35
Glue 2, RT curing	~50
Glue 2, 40°C curing	70+
Glue 3, RT curing	~55
Glue 3, 40°C curing	~55

*The effective Tg includes the layer thickness, which a true Tg would not

Table 3: Temperature performances resulting from the Tg test

6.1.2 Tg test discussion

The actuators are heated by convection created by the heatplate. The bottom element will receive more of the convection heating than the top element, which might amplify the tip displacement. Both aluminium and silicon are excellent heat conductors and the elements and adhesive layer are very thin, therefore, the problem will most likely be minimal. On top of that this test gives a relative measurement between the samples. The effect caused by this error would only change the slope of the tip displacement plot, which will not have any influence on the results. Whether this error is actually occurring could be tested by measuring an actuator with two aluminium elements. If there is a difference in temperature between the elements this actuator will have a displacement. However, as this error should not influence relative measurements this test has not been conducted.
As mentioned in table 3 not the actual Tg but the effective Tg is measured. Meaning, that this experiment measures the bonding strength instead of the adhesive strength. However, as the bonding strength is the value that is relevant for this research only the term that is used is incorrect.
The ideal case in the tip displacement plots shows the calculated displacement using equation 6. It is expected that the actual elements will have a smaller slope than this ideal case, as was shown in the Comsol calculation of figure 45. However this calculation showed a decrease in slope of about 10% instead of the measured 30%. There are a few potential causes for the difference between calculation and measurement. First the Youngs modulus of the adhesives could be lower than the values used in Comsol (the calculation used an average value for adhesives as the adhesive datasheets do not provide a clear value). Another explanation could be improper compression of the adhesive layer. The aluminium elements were not perfectly flat and during curing they were compressed with about 0.5kg. Possibly the glue has not attached properly causing a weaker bonding.

6.1.3 Tg test recommendations for further testing

To properly confirm whether the adhesives will hold tests should be conducted with an environmentally controlled tensile testing machine. The current Tg test can be used to find the best suited adhesives, but it will not result in an absolute value confirming whether the adhesive will survive the high transport temperatures.

6.2 Drift test

For each of the 8 combinations 3 samples are constructed (for a total of 24 samples). The samples are measured every Monday morning for about 2 months.

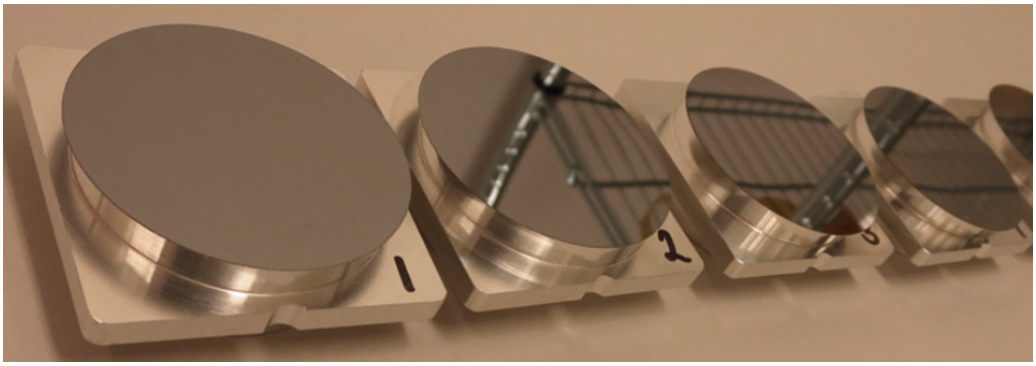

Figure 62: First batch of drift test samples

6.2.1 Validation

The budget for the bow error is limited to a few micrometer, therefore the bow error caused by the drift has to be measured at a sub-micrometer accuracy. To ensure that this accuracy is reached the measurement method has to be validated.
First the shape of the curves are evaluated. The height maps of the first sample in the first week can be seen in figure 63. After the plane compensation the shape is roughly what is expected with the deepest point of the bow within 10% of the calculated value. However, the location of the lowest point is located slightly off-centre (this was roughly the same for all samples). The samples are measured by docking them against the 3 pins of the sample holder, this ensures that the same position is measured with every measurement. The most likely cause of the shifted lowest point is that the original centre location was wrong, which causes every measurements lowest point to be a bit off. However, as the measurements are identically repeated this should not influence the drift measurement.

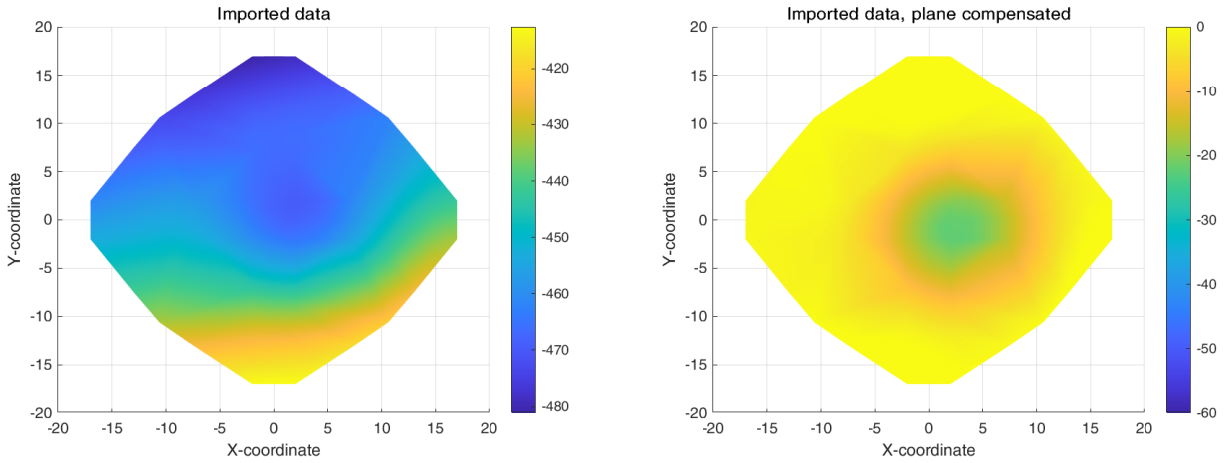

(a) Height map raw data

(b) Height map plane compensated data

Figure 63: Height maps before and after plane compensation of sample 1, units removed for IP purposes

The next validation is the reproducibility of the height measurements, when the same sample is measured multiple times in succession the result should be the same. A sample was measured 5 consecutive times in 5 sessions. For 2 of these sessions the sample was replaced on the stage by hand between the measurements, for 3 sessions the sample was left on the stage. The reproducibility measurements can be seen in figure 64.

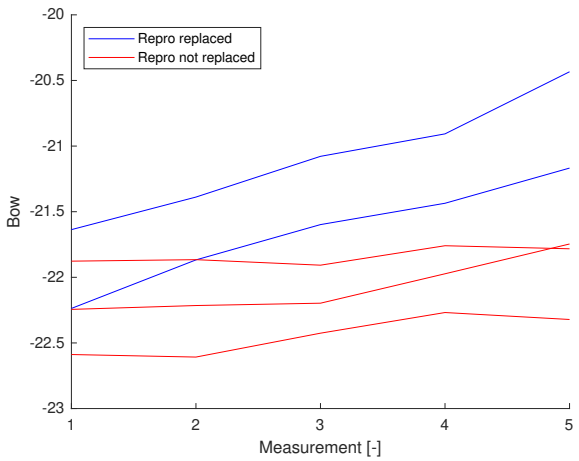

Figure 64: 5-measurement reproducibility test (measurements were conducted in different weeks)

the standard deviation of the measurement without replacing the sample between the measurements is at an acceptable level, the deviation when the samples are replaced is too high. However, the deviation of all 5 measurements is not random, the bow is steadily decreasing in size. As mentioned in the design of the drift experiment in chapter 5 the difference in CTE between silicon and aluminium prevented any higher temperature curing. It is hypothesised that this difference in CTE is also the cause for the shift in the measurement. When the samples heat up, the aluminium spacer will expand more than the silicon element, causing the tension in the element to increase. The increased tension in the element will straighten it, decreasing the bow (which is seen in the measurements).
If the hypotheses above is true something causes the samples to heat up during the replacement and during the measurement. There are two sources that are suspected to cause the sample to heat up, the hands of the operator during replacement and the stage during the measurement.

To confirm whether the hands of the operator are the source of the reproducibility error a test is conducted where the sample is replaced on the stage using different methods. First the sample is replaced using tools (preventing heat transfer from the operator's hands), next the sample is regularly handled by the operator and lastly the sample is regularly replaced but very slowly (allowing more heat transfer from the operator's hands). If the hypothesis is true the bow should be stable when handled by tools, decrease when handled by the operator and decrease faster when slowly handled by the operator. The results from this test can be seen in figure 65 (note that an upwards curve is a decreasing bow).

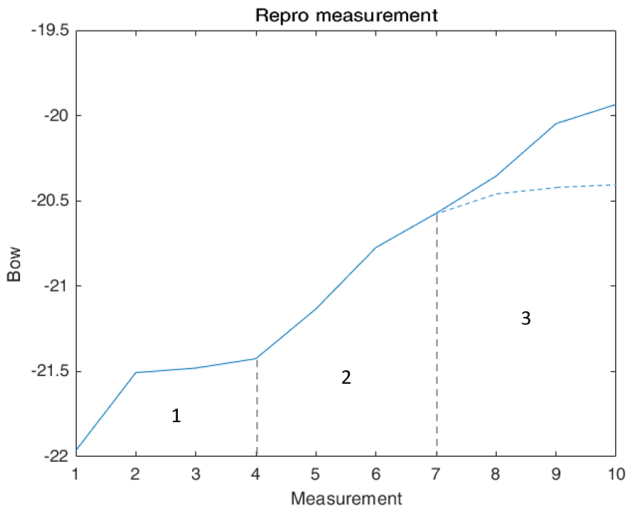

Figure 65: Replacement reproducibility test

In area 1 the bow decreases rapidly with the first measurement as the sample reaches the stage temperature, afterwards the bow is steady (as expected with tool replacement). Between the measurements in area 2 the sample is touched by the operator's hands, which can be seen in by the decreasing bow. The blue striped line indicates the expected progress of the bow, as the sample temperature will reach a steady state between the warm operator's hands and the cool stage. Between the measurements in area 3 the sample is replaced slowly, allowing more heat transfer to the samples. This would result in a new steady state with a smaller bow, which can also be seen in the measurements.
This test shows that the operator's hands are indeed the heat source causing the reproducibility error. However, as all samples are handled identically during the measurements, this error should not show in the drift measurements.

It is hypothesised that the stage is the second heat source causing the smaller reproducibility error for the samples without replacement. During a measurement the XY stage moves the sample to 273 separate points in about 7 minutes. The electric motors that power the stage will heat up during this movement and could potentially cause the stage to heat up with it. To confirm whether the stage is the source of the heat a long interval reproducibility test is proposed. The reproducibility measurements are repeated, but this time at one hour intervals to allow the stage to cool off between the measurements.

If the stage is the primary heat source the measurements should have a relatively good reproducibility, this was however not the case. The measurements showed an error at the timescale of several hours. Although the stage is most likely not the source of this error, it is expected that temperature differences are still the cause. When the temperature increases the bow should decrease, in figure 66 the cleanroom temperature and element bow are plotted together against time. It can be seen that the element bow roughly follows the cleanroom temperature with some delay.

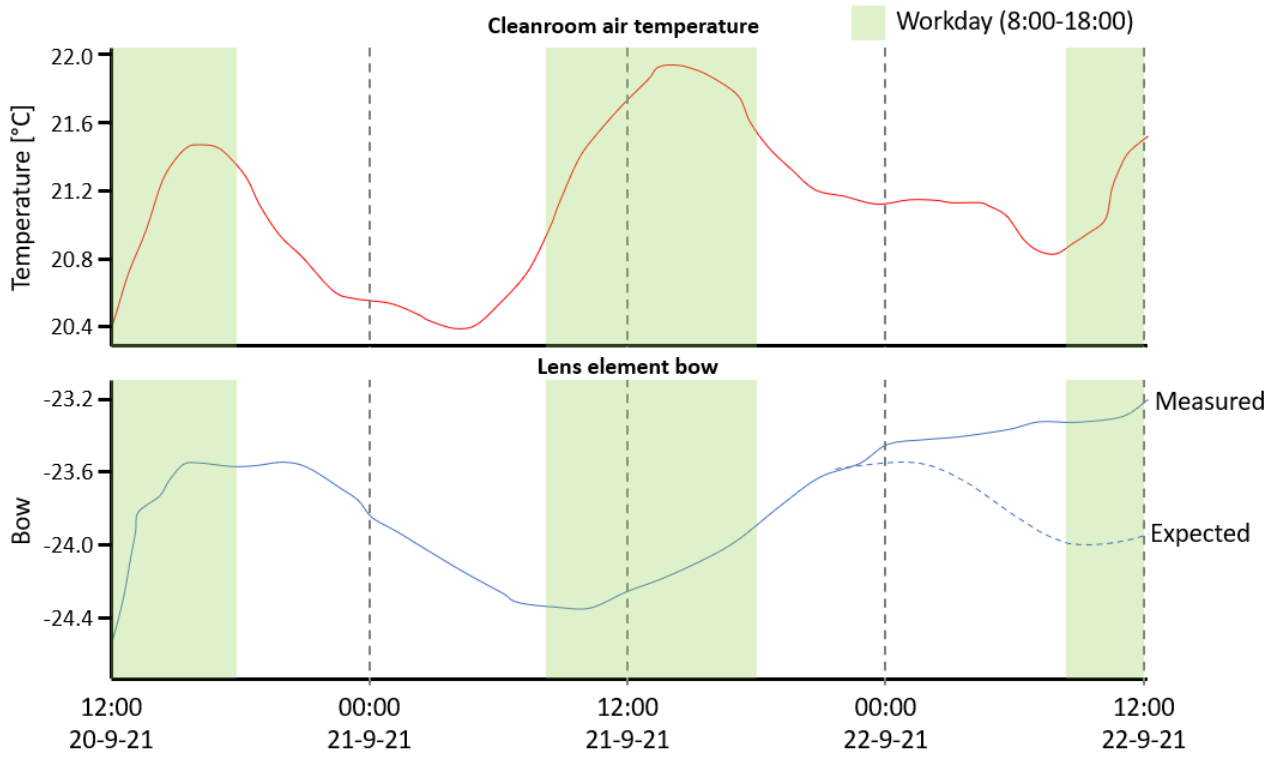

Figure 66: 48 hour reproducibility test

There is one deviation in the measured curve with respect to the expected curve. At the end of the measurement the temperature decreased while the measured bow stabilised. The most likely explanation is a measurement error in the temperature sensor. Due to the location of the temperature sensor in the ventilation system, differences in humidity can change the temperature which will not show on the sensor. Due to the error in the system the temperature sensor only provides a rough estimate of the temperature.
Although the primary source of the error is most likely not the heating of the stage but the changing cleanroom temperature, the dependence between element bow and temperature is proven.

6.2.2 Results

For the drift test a total of 24 samples are build using 3 samples for each of the following combination of adhesive, curing and additives:

Batch	Adhesive	Curing	Additives
1a	Glue 2	Room temperature	50µm beads
1b	Glue 3	Room temperature	50µm beads
2a	Glue 2	30°C	50µm beads
2b	Glue 3	30°C	50µm beads
3a	Glue 1	Room temperature	50µm beads
3b	Glue 1	Room temperature	No beads
3c	Glue 1	30°C	50µm beads
3d	Glue 1	30°C	No beads

Table 4: Drift sample combinations

As explained in the design of experiment the drift samples are cured at 30°C instead of the 40°C used for the Tg test. The lower temperature requires a longer curing time. In accordance with the datasheets the curing time was increased by 50% with respect to the used 40°C curing time. Unfortunately batch 3b failed during production. The samples have been produced at a rate of one batch per week, resulting in a smaller amount of measurements for the latter batches. Every Monday morning the samples are measured at roughly the same time and the temperature is noted. The data set resulting from the measurement is processed in Matlab and the lowest point in the bow is calculated. To properly show the change in bow the size of the first measurement is subtracted from the data set. As each combination has 3 samples the data is averaged for each combination. The results of the drift measurements can be seen in figure 67.

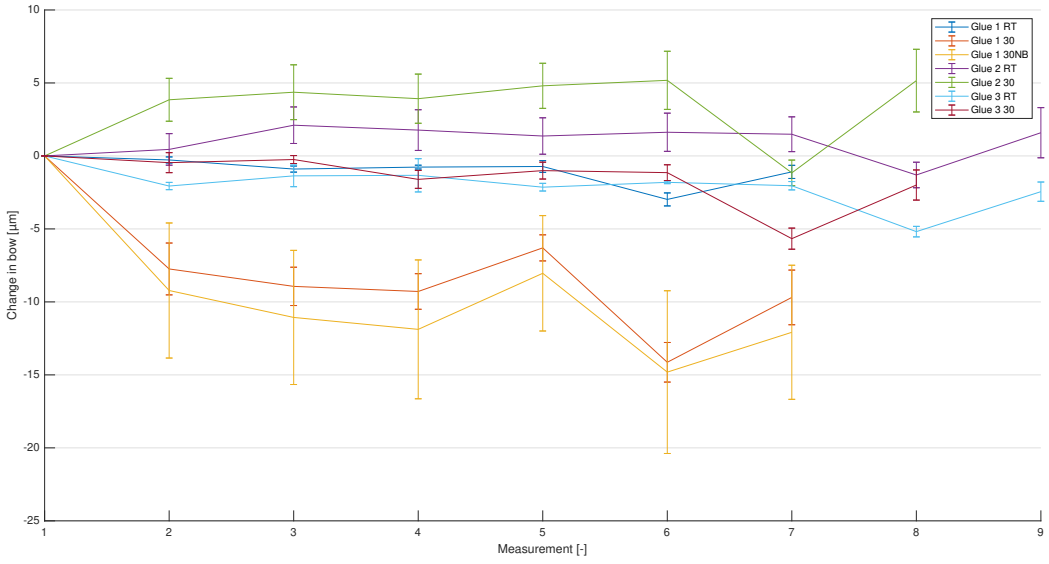

Figure 67: Drift measurements, aligned by starting point

The Tg measurements showed that glue 1 performs the worst with increased temperature. This can also clearly be seen in the drift measurements of figure 67, where the drift of these combinations performed significantly worse than the other samples. The absolute bow of these samples is larger than the others, likely caused by the adhesive not being able to hold the element in place at the higher curing temperature. On top of that that the samples without beads are very unreliable due to the large error bars. To better evaluate the results from the other adhesives the figure has been plotted without these 2 combinations in figure 68.

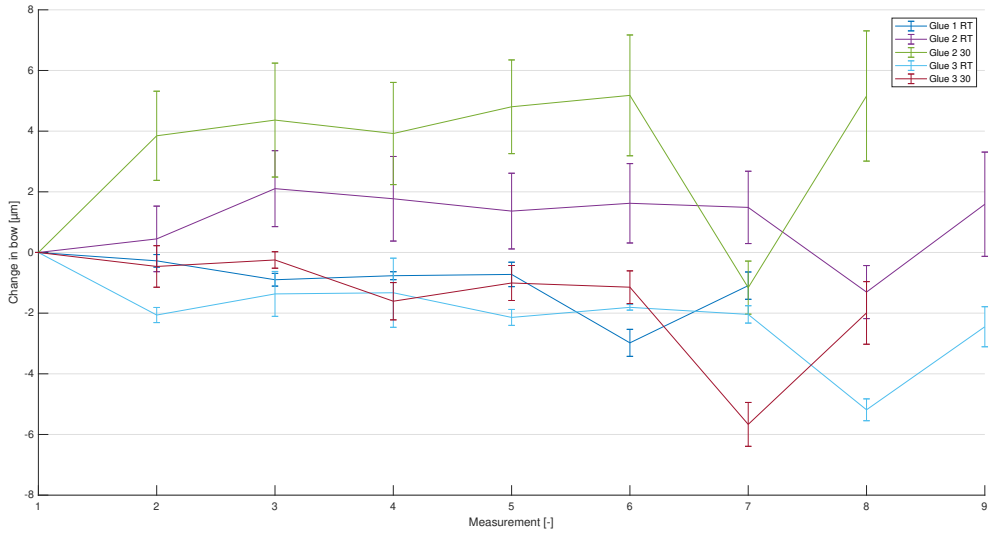

Figure 68: Drift measurements without glue 1 30°C curing, aligned by starting point

Most of the adhesives in figure 68 show the largest amount of drift in the first week and seem to stabilise after the first 2 weeks, except for a large valley for every sample after 6 to 8 weeks. To properly show the drift effects of the first 2 weeks to measurement are aligned to all start at the same point. Therefore, in this graph when two measurements have the same number, it does not necessarily mean they were measured at the same time. When the measurements are aligned by the week they are measured and not their starting point the figure changes, see figure 69.

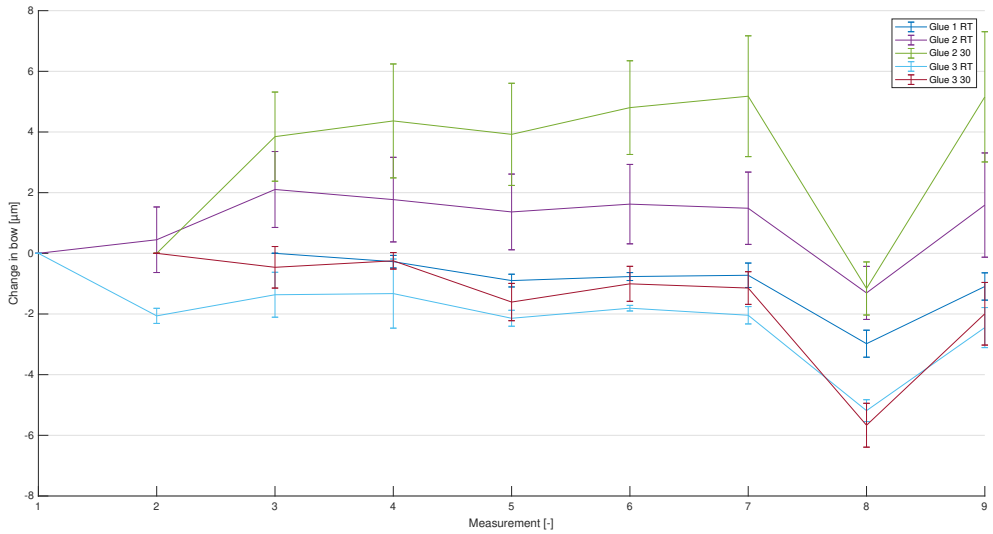

Figure 69: Drift measurements without glue 1 30°C curing, aligned by measurement date

In the 8th week of the measurements the bow of every sample decreases significantly. The measurements are conducted every Monday morning, therefore, the problem has most likely occurred during the weekend. In the validation it was already confirmed that the samples are dependent on temperature. To check whether the CTE difference is indeed the cause of this error the temperature of the cleanroom over the weekend is checked. It turned out that the temperature control of the cleanroom had failed over the weekend, causing the temperature to drop to 19.3°C on Sunday night (while the allowed minimum is 20.5°C). The cold samples caused the bow to increase, which can clearly be seen in the figure. This further confirms the hypotheses that the reproducibility errors are due to temperature and CTE differences.

When the measurements from week 8 are removed from the graph the drift test shows a clear pattern. Generally, a relatively large amount of drift is measured in the first 2 weeks which stabilises over time. To show the performance of the adhesives the occurred drift of the latest measurement is shown in table 5. The amount of weeks that the samples have been measured is different for each batch. Therefore, the results that are shown in the table are not for exactly the same amount of weeks of drift. However, as the drift stabilises the measurements do not change significantly for the last weeks of measurements. Therefore, the latest measurements still give a good indication of the occurred drift.

Combination	Error caused by drift [µm]	Measured weeks
Glue 1, RT curing	-1.1	7
Glue 1, 30°C curing	-9.7	7
Glue 1, RT curing, no beads	Failed samples	-
Glue 1, 30°C curing, no beads	-12.1	7
Glue 2, RT curing	1.6	9
Glue 2, 30°C curing	5.2	8
Glue 3, RT curing	-2.4	9
Glue 3, 30°C curing	-2.0	8

Table 5: Drift performances resulting from the drift test

6.2.3 Drift test discussion

The large temperature dependence of the samples does present a problem, how valid are the measurements when environmental parameters have such a large effect? The effect of the temperature is roughly the same for every sample. Therefore, the environmental temperature can only be the cause of an error when all the samples show the same behaviour. This can be seen to a large degree on week 8, but also to a smaller degree on week 5. In this week all samples show a small increase in bow, indicating that the samples were slightly colder. However, as the behaviour of the samples does not seem to be dependant on each other for the remaining measurements, the effect of environmental temperature will likely not be dominant.

In the experiment design of chapter 5 the ratio between lateral drift and bow error are calculated. These values were in the thousands, meaning that if the bow would increase by a micrometer only a nanometer of lateral movement in the bonding is required. Using this relation the temperature change required to cause the bow measured in week 8 is about a one hundredth of a degree Celsius, which is not realistic. However, the situation where the lateral movement is caused by thermal shrink of the element holder is a different situation. In this case compressive forces push on the sides of the element and result in an increase in bow (see figure 70). However, the force required to compress a near flat element is large. Due to the large forces a significant share of lateral movement is absorbed by the compression of the silicon element and elasticity of the adhesive layer. Together these factors reduce the ratio of lateral drift and change in bow to about ten, instead of a few thousand. Using the factor of ten the bow seen in the drift measurement requires a decrease in temperature of about 1.5°C, which roughly matches the measured temperature change in the cleanroom.

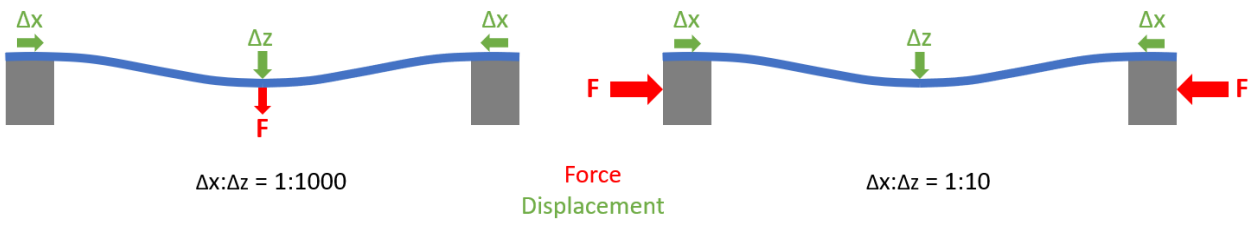

Figure 70: The ratio of drift to sag depends on the application of the force

The last observation from the test that should be discussed is the decreasing bow of glue 2. While both glue 1 and 3 with both curing processes had increasing bows (as expected), glue 2 has a decreasing bow over time for both cures. Meaning, that glue 2 is actually pulling the weight upwards by decreasing the bow of the element over time. A potential explanation for the decrease in bow could be adhesive shrink. Due to applied load the adhesive will be stretched diagonally while the beads prevent the elements to move closer to each other. When the diagonally stretched adhesive shrinks it can apply a lateral force on the element, decreasing the bow (see figure 71). If this hypotheses is true glue 2 would requires almost 2 weeks for curing and exhibits significant shrink during curing, which should be taken into account.

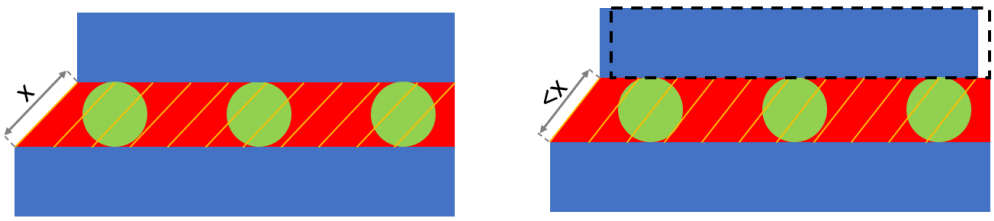

Figure 71: Adhesive shrink can be a potential cause for a decreasing bow

In the design of the experiments some large simplifications were made to make the experiment feasible in the available time frame (no hole grid and a point load instead of a distributed load). When the element has a higher stiffness it reduces the shear load on the bonding. A different type of load changes the shape of the curve which will also influence the shear load on the bonding. For more accurate tests less simplifications should be used.

6.2.4 Drift test recommendations for further testing

It was observed that the test setup was sensitive to temperature due to the CTE differences between the element holder and element. The easiest way to fix this problem is by machining the element holder out of borosilicate glass. This is however rather expensive and time consuming. Another possible fix would be to add an intermediate layer between the element and element holder (see figure 72). The lens element would be glued to a borosilicate ring, which would be laid down on top of an aluminium holder. The aluminium holder will be slightly oversized (about 0.1mm), preventing the borosilicate ring from freely moving around. If the sample would heat up, the aluminium holder will expand more than the borosilicate ring, but it will not apply any force on the silicon element. This setup would allow for higher curing temperatures and will most likely eliminate the temperature dependency of the setup.

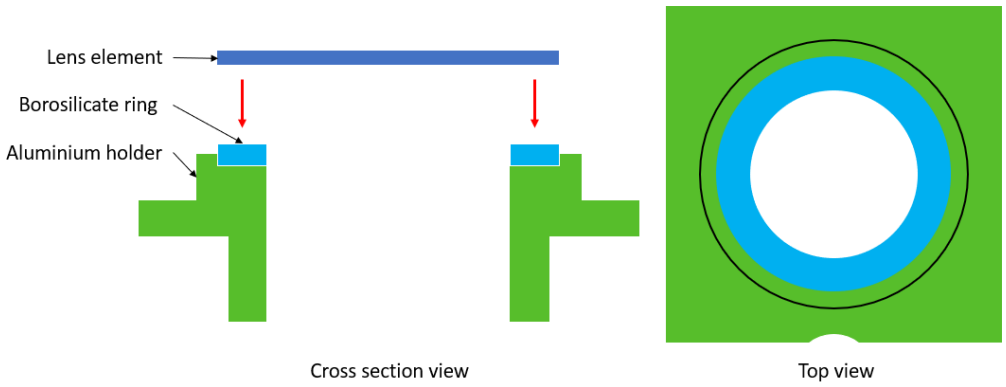

Figure 72: Improved drift test setup for less temperature sensitivity

It is also seen that the majority of drift occurs in the first two weeks. Therefore it is advisable to have a higher measurement frequency in the first two weeks. Potentially a single sample could be placed in the measuring setup while running the measuring script every hour for the first two weeks. Together with the less temperature sensitive drift setup this could give a very clear image on the occurring drift.

The SEM containing the lenses will not always be turned on. When the machine is turned off the potential difference between the lens elements will disappear, thus the load will be removed. If the drift is reversible, meaning that the lens elements will return to their original position (before the drift) when the electric field is removed, the drift will start again when the electric field is turned on again. Preferably the drift is irreversible, meaning that if the electric field is turned off the occurred drift does not return. To test whether the drift is irreversible a setup should be designed where the load can be removed from the sample. This can potentially be tested with the current samples by flipping them upside down for several weeks (see figure 73). However, this not only removes the downwards force but also introduces a force pushing the elements flat again. Therefore, it would be better to properly design a setup to test this.

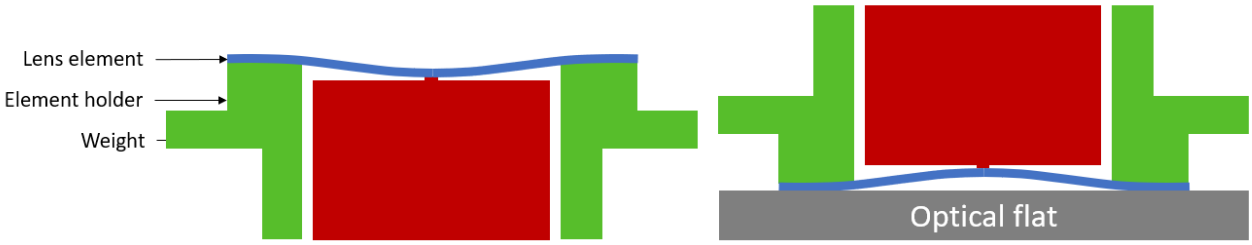

Figure 73: Reversed drift can be tested by flipping the samples upside down

6.3 Experiment conclusion

The experiments have two goals, firstly to select which combination of adhesives, curing and layer thickness yield the best result and secondly an estimation of the expected size of the errors caused by the bonding. The results for both tests are plotted in table 6.

Combination	Tg Test [°C]	Drift test [µm]
Glue 1, RT curing	~45	-1.1
Glue 1, 30/40°C curing	70+	-9.7
Glue 1, RT curing, no beads	~40	Failed samples
Glue 1, 30/40°C curing, no beads	~35	-12.1
Glue 2, RT curing	~50	1.6
Glue 2, 30/40°C curing	70+	5.2
Glue 3, RT curing	~60	-2.4
Glue 3, 30/40°C curing	~60	-2

Table 6: Performances resulting from both tests

Glue 1 and 2 both perform well on the drift test when cured at room temperature. However they both require a higher temperature cure to reach a proper Tg. The best overall performing adhesive is glue 3, with both curing temperatures it had good results on both tests.
The Tg test is conducted to evaluate whether a lens stack would survive the transport with extreme temperatures. However, as special transport requests can be made this requirements has a lower priority than the drift requirement.
Based on the importance of Tg relative to drift an adhesive can be chosen. If the best overall specifications are desired glue 3 is recommended. If the best drift performance is desired glue 1 with a room temperature curing is recommended (although glue 2 with a room temperature curing is not far behind).

7 Discussion

Some bonding methods in chapter 3.1 were dropped due to the limited available time. Although surface activated bonding is sensitive to particles and CTE differences the methods is still very promising. If more time and sufficient budget is available it would be interesting to properly research this method of bonding.
Whether the budget of an error category is met depends on the tolerances reached on the elements like TTV, hole sizes and many other parameters. The tolerances on these parameters are very tight and especially the combination of all these tolerances can be a challenge. Whether the assumption that all of them can be met simultaneously is true will have to be proven in practice.
The Tg test of chapter 5 gives a good indication for the performance of the adhesives with temperature. However, it does not guarantee whether a lens element could survive the maximum transport temperature. To test this an absolute measurement should be conducted with an environmentally controlled tensile testing machine, or a stack should be heated to 60°C and have the tolerances checked before and after. The drift test gave a good indication on the expected bow errors due to drift. However the values are slightly distorted due to many simplifications and CTE errors. The simplifications cause the situation to change due to different element stiffness and loads (although according to the calculations the test setup should be worse than the actual case). On top of that the difference in CTE causes measurement errors and will most likely caused additional forces and errors on the higher temperature cured samples.

8 Conclusion

In the trade-offs introduced in chapter 3 the preferred method of bonding is selected. It was concluded that adhesive bonding is the most promising bonding method for this research and in the following trade-off the best suited adhesives are selected.
From the analysis conducted in chapter 4 it can be concluded that it is not feasible to reach the required focal plane flatness with the initial requirements. However, by changing some of the boundary conditions and introducing additional methods of error compensation the focal plane flatness can stay within budget. With these changes about half of the budget is needed for the calculated errors while the other half is saved for the expected adhesive bonding errors.
The glass transition temperature test explained in chapter 5 showed that for glue 1 and glue 2 increasing the post curing temperature significantly increased the glass transition temperature. The increase in Tg with a higher post curing temperature was however barely seen for glue 3. If higher curing temperatures can be used both glue 1 and 2 perform very well, if room temperature curing is required glue 3 is the best performing adhesive. The test also showed that even when the datasheets provide a comparable Tg, the actual results can differ.
The drift test described in chapter 5 showed that glue 1 is the best performing adhesive for the smallest drift error and that glue 2 most likely requires more than a week to fully cure. The test also showed that the majority of drift occurs in the first two weeks after the load is applied. For the best performing adhesives the drift error of the first 2 months just fits in the assigned error budget. However, the remaining drift after the initial two weeks is stabilising. Therefore, if the initial drift can be compensated in the systematic bow error, the requirements for the lens stack seem to be feasible. Whether the initial drift can be compensated in the systematic bow error depends on the reversibility of the drift. To test this another experiment is proposed in the recommendations for further testing in chapter 6.

9 Acknowledgement

Throughout my thesis I received a lot of support from the people around me. Their support has helped and motivated me to give my best effort for this report.

I would first like to thank my supervisors, Hans van Gurp and Jo Spronck. Hans has supported me for over a year with technical insights, planning, feedback and some occasional terrible humor. Jo has provided me with many technical insights, pushed me to challenge the people around me and gave me the freedom to structure this research in a way that fits the subject.

I would also like to thank my parents, who have supported me throughout my entire life. They have always been there for me and have given invaluable advice throughout my career and this thesis.

Finally I would like to thank Dennis Seekles, Paul Scheffers, Marco Wieland, Jurgen van Soest, Joost Koning, Laura Dinu Gurtler, Michiel Bruinink and the rest of my team at ASML. For every issue I encountered I could always count on my team to help me out.

References

[1] ASML. *Moore's law*. 2021. URL: https://www.asml.com/en/technology/all-about-microchips/moores-law.

[2] Technik Consulting. *Bimetallic actuator calculator*. 2021. URL: https://www.technik-consulting.eu/en/science/bimetal.html.

[3] V. Dragoi and E. Pabo. "Wafer bonding technology for new generation vacuum MEMS: challenges and promises". In: *Smart Sensors, Actuators, and MEMS VII; and Cyber Physical Systems*. Ed. by José Luis Sánchez-Rojas and Riccardo Brama. Vol. 9517. International Society for Optics and Photonics. SPIE, 2015, pp. 43–50. URL: https://doi.org/10.1117/12.2178920.

[4] Engineering Fundamentals. *Circular clamped plate under uniformly distributed load*. 2021. URL: https://www.efunda.com/formulae/solid_mechanics/plates/calculators/cpC_PUniform.cfm.

[5] B.J. Inkson. "2 - Scanning electron microscopy (SEM) and transmission electron microscopy (TEM) for materials characterization". In: *Materials Characterization Using Nondestructive Evaluation (NDE) Methods*. Ed. by Gerhard Hübschen et al. Woodhead Publishing, 2016, pp. 17–43. ISBN: 978-0-08-100040-3. DOI: https://doi.org/10.1016/B978-0-08-100040-3.00002-X. URL: https://www.sciencedirect.com/science/article/pii/B978008100040300002X.

[6] K. Krishnakumar and A. John. "Determination of Effective Thermal Conductivity of Perforated Plates with Low Porosities Used as Matrix Heat Exchanger Core Surfaces". In: 2015.

[7] C.C. Lee, C.Y. Wang, and G. Matijasevic. "Au-In bonding below the eutectic temperature". In: *IEEE Transactions on Components, Hybrids, and Manufacturing Technology* 16.3 (1993), pp. 311–316. DOI: 10.1109/33.232058.

[8] Syed P.S. "Phase Rule CHAPTER-6 PHASE RULE". In: Oct. 2010, 6.1 to 6.26.

[9] Thomas Plach et al. "Chapter 23 - Silicon direct bonding". In: *Handbook of Silicon Based MEMS Materials and Technologies (Third Edition)*. Ed. by Markku Tilli et al. Third Edition. Micro and Nano Technologies. Elsevier, 2020, pp. 567–580. ISBN: 978-0-12-817786-0. DOI: https://doi.org/10.1016/B978-0-12-817786-0.00023-2. URL: https://www.sciencedirect.com/science/article/pii/B9780128177860000232.

[10] Thomas Plach et al. "Chapter 23 - Silicon direct bonding". In: *Handbook of Silicon Based MEMS Materials and Technologies (Third Edition)*. Ed. by Markku Tilli et al. Third Edition. Micro and Nano Technologies. Elsevier, 2020, pp. 567–580. ISBN: 978-0-12-817786-0. DOI: https://doi.org/10.1016/B978-0-12-817786-0.00023-2. URL: https://www.sciencedirect.com/science/article/pii/B9780128177860000232.

[11] Fred Roozeboom et al. "Cyclic Etch/Passivation-Deposition as an All-Spatial Concept toward High-Rate Room Temperature Atomic Layer Etching". In: *ECS Journal of Solid State Science and Technology* 4 (Feb. 2015), N5067–N5076. DOI: 10.1149/2.0111506jss.

[12] Hideki Takagi et al. "Low-temperature direct bonding of silicon and silicon dioxide by the surface activation method". In: *Sensors and Actuators A: Physical* 70.1 (1998), pp. 164–170. ISSN: 0924-4247. DOI: https://doi.org/10.1016/S0924-4247(98)00128-9. URL: https://www.sciencedirect.com/science/article/pii/S0924424798001289.

[13] Testomatric. *Tensile testers*. 2021. URL: http://www.testometric.co.uk/50kn/.

[14] Amirkoushyar Ziabari, Zhixi Bian, and Ali Shakouri. "Adaptive Power Blurring Techniques to Calculate IC Temperature Profile under". In: *Large Temperature Variations, International Microelectronic and Packaging Society (IMAPS) ATW on Thermal Management*, pp. 28–30.